Title: The potassium channel subunit $K_V1.8$ (*Kcna10*) is essential for the distinctive outwardly rectifying conductances of type I and II vestibular hair cells

Hannah R. Martin[1], ORCID 0000-0003-2028-5798
Anna Lysakowski[2], ORCID 0000-0001-6259-0294
Ruth Anne Eatock[1], ORCID 0000-0001-7547-2051

[1]University of Chicago, Department of Neurobiology
[2]University of Illinois at Chicago, Department of Anatomy and Cell Biology

Author for correspondence:
Ruth Anne Eatock
Dept of Neurobiology, J251
University of Chicago
Chicago, IL
eatock@uchicago.edu

Keywords: potassium channels, hair cells, vestibular, inner ear, receptor potential

Abstract

In amniotes, head motions and tilt are detected by two types of vestibular hair cells (HCs) with strikingly different morphology and physiology. Mature type I HCs express a large and very unusual potassium conductance, $g_{K,L}$, which activates negative to resting potential, confers very negative resting potentials and low input resistances, and enhances an unusual non-quantal transmission from type I cells onto their calyceal afferent terminals. Following clues pointing to $K_V1.8$ (KCNA10) in the Shaker K channel family as a candidate $g_{K,L}$ subunit, we compared whole-cell voltage-dependent currents from utricular hair cells of $K_V1.8$-null mice and littermate controls. We found that $K_V1.8$ is necessary not just for $g_{K,L}$ but also for fast-inactivating and delayed rectifier currents in type II HCs, which activate positive to resting potential. The distinct properties of the three $K_V1.8$-dependent conductances may reflect different mixing with other K_V subunits that are reported to be differentially expressed in type I and II HCs. In $K_V1.8$-null HCs of both types, residual outwardly rectifying conductances include K_V7 (KCNQ) channels.

Current clamp records show that in both HC types, $K_V1.8$-dependent conductances increase the speed and damping of voltage responses. Features that speed up vestibular receptor potentials and non-quantal afferent transmission may have helped stabilize locomotion as tetrapods moved from water to land.

Graphical abstract

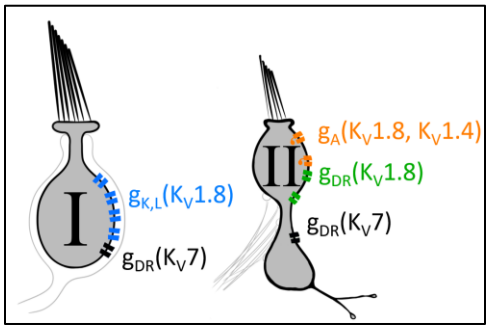

Abbreviations:

g_A, A-type (inactivating) K_V conductance in type II HCs

g_{DR}, delayed rectifier K^+ conductance

$g_{K,L}$, low-voltage-activated K^+ conductance in type I HCs

HC, hair cell

K_V, voltage-gated K^+ conductance

Introduction

The receptor potentials of hair cells (HCs) are strongly shaped by large outwardly rectifying K^+ conductances that are differentially expressed according to HC type. Here we report that a specific voltage-gated K^+ (K_V) channel subunit participates in very different K_V channels dominating the membrane conductances of type I and type II HCs in amniote vestibular organs.

Type I HCs occur only in amniote vestibular organs. Their most distinctive features are that they are enveloped by a calyceal afferent terminal (Wersäll, 1956; Lysakowski and Goldberg, 2004) and that they express $g_{K,L}$ (Correia and Lang, 1990; Rennie and Correia, 1994; Rüsch and Eatock, 1996a): a large non-inactivating conductance with an activation range from –100 to –60 mV, far more negative than other "low-voltage-activated" K_V channels. HCs are known for their large outwardly rectifying K+ conductances, which repolarize membrane voltage following a mechanically evoked perturbation and in some cases contribute to sharp electrical tuning of the hair cell membrane. $g_{K,L}$ is unusually large and unusually negatively activated, and therefore strongly attenuates and speeds up the receptor potentials of type I HCs (Correia et al., 1996; Rüsch and Eatock, 1996b). In addition, $g_{K,L}$ augments non-quantal transmission from type I HC to afferent calyx by providing open channels for K^+ flow into the synaptic cleft (Contini et al., 2012, 2017, 2020; Govindaraju et al., 2023), increasing the speed and linearity of the transmitted signal (Songer and Eatock, 2013).

Type II HCs have compact afferent synaptic contacts (boutons) where the receptor potential drives quantal release of glutamate. They have fast-inactivating (A-type, g_A) and delayed rectifier (g_{DR}) conductances that are opened by depolarization above resting potential (V_{rest}).

The unusual properties of $g_{K,L}$ have long attracted curiosity about its molecular nature. $g_{K,L}$ has been proposed to include "M-like" K_V channels in the K_V7 and/or erg channel families (Kharkovets et al., 2000; Hurley et al., 2006; Holt et al., 2007). The $K_V7.4$ subunit was of particular interest because it contributes to the low-voltage-activated conductance, $g_{K,n}$, in cochlear outer hair cells, but was eventually eliminated as a $g_{K,L}$ subunit by experiments on $K_V7.4$-null mice (Spitzmaul et al., 2013).

Several observations suggested the $K_V1.8$ (KCNA10) subunit as an alternative candidate for $g_{K,L}$. $K_V1.8$ is highly expressed in vestibular sensory epithelia (Carlisle et al., 2012), particularly hair cells (Lee et al., 2013; Scheffer et al., 2015; McInturff et al., 2018), with slight expression elsewhere (skeletal muscle, Lee et al., 2013; kidney, Yao, 2002). $K_V1.8^{-/-}$ mice show absent or delayed vestibular-evoked potentials, the synchronized activity of afferent nerve fibers sensitive to fast linear head motions (Lee et al., 2013). Unique among K_V1 channels, $K_V1.8$ has a cyclic nucleotide binding domain (Lang et al., 2000) with the potential to explain $g_{K,L}$'s known cGMP dependence (Behrend et al., 1997; Chen and Eatock, 2000).

Our comparison of whole-cell currents and immunohistochemistry in type I HCs from $K_V1.8^{-/-}$ and $K_V1.8^{+/+,+/-}$ mouse utricles confirmed that $K_V1.8$ expression is necessary for $g_{K,L}$. More surprisingly, $K_V1.8$ expression is also required for A-type and delayed rectifier conductances of type II HCs. In both HC types, eliminating the $K_V1.8$-dependent major conductances revealed a smaller delayed rectifier conductance involving K_V7 channels. Thus, the distinctive outward rectifiers that produce such different receptor potentials in type I and II HCs both include $K_V1.8$ and K_V7 channels.

Results

We compared whole-cell voltage-activated K^+ currents in type I and type II hair cells from homozygous knockout ($K_V1.8^{-/-}$) animals and their wildtype ($K_V1.8^{+/+}$) or heterozygote ($K_V1.8^{+/-}$) littermates. We immunolocalized $K_V1.8$ subunits in the utricular epithelium and pharmacologically characterized the residual K^+ currents of $K_V1.8^{-/-}$ animals. Current clamp experiments demonstrated the impact of $K_V1.8$-dependent currents on passive membrane properties.

We recorded from three utricular zones: lateral extrastriola (LES), striola, and medial extrastriola (MES) (Fig. 3A.1); striolar and extrastriolar zones have many structural and functional differences and give rise to afferents with different physiology (reviewed in Goldberg, 2000; Eatock and Songer, 2011). Recordings are from 412 type I and II HCs (53% LES, 30% MES, 17% striola) from mice between postnatal day (P) 5 and P370. We recorded from such a wide age range to test for developmental or senescent changes in the impact of the null mutation. Above P18, we did not see substantial changes in K_V channel properties, as reported (González-Garrido et al., 2021).

$K_V1.8^{-/-}$ animals appeared to be healthy and to develop and age normally, as reported (Lee et al., 2013), and hair cells were healthy (see Methods for criteria).

$K_V1.8$ is necessary for $g_{K,L}$ in type I hair cells

The large low-voltage activated conductance, $g_{K,L}$, in $K_V1.8^{+/+,+/-}$ type I hair cells produces distinctive whole-cell current responses to voltage steps, as highlighted by our standard type I voltage protocol (Fig. 1A). From a holding potential within the $g_{K,L}$ activation range (here –74 mV), the cell is hyperpolarized to –124 mV, negative to E_K and the activation range, producing a large inward current through open $g_{K,L}$ channels that rapidly decays as the channels deactivate. We use the large transient inward current as a hallmark of $g_{K,L}$. The hyperpolarization closes all channels, and then the activation function is probed with a series of depolarizing steps, obtaining the maximum conductance from the peak tail current at –44 mV (Fig. 1A). We detected no difference between the Boltzmann parameters of $g_{K,L}$ G-V curves from $K_V1.8^{+/-}$ and $K_V1.8^{+/+}$ type I HCs.

For a similar voltage protocol, $K_V1.8^{-/-}$ type I HCs (Fig. 1B) produced no inward transient current at the step from –74 mV to –124 mV and much smaller depolarization-activated currents during the iterated steps, even at much more positive potentials. Figure 1C compares the conductance-voltage (G-V, activation) curves fit to tail currents (Eq. 1; see insets in Fig. 1A-B): the maximal conductance (g_{max}) of the $K_V1.8^{-/-}$ HC was over 10-fold smaller (Fig. 1C.1), and the curve was positively shifted by >40 mV (Fig. 1C.2). Figure 1D shows the G-V Boltzmann fit parameters for type I HCs from mice >P12, an age at which type I HCs normally express $g_{K,L}$ (Rüsch et al., 1998).

Suppl. Fig. 1 shows how G-V parameters of outwardly rectifying currents in type I HCs changed from P5 to P360. In $K_V1.8^{+/+,+,-}$ mice, the parameters transitioned over the first 15-20 postnatal days from values for a conventional delayed rectifier, activating positive to resting potential, to $g_{K,L}$ values, as previously described (Rüsch et al., 1998; Géléoc et al., 2004; Hurley et al., 2006). Between P5 and P10, some type I HCs have not yet acquired the physiologically defined conductance, $g_{K,L}$. No effects of $K_V1.8$ deletion were

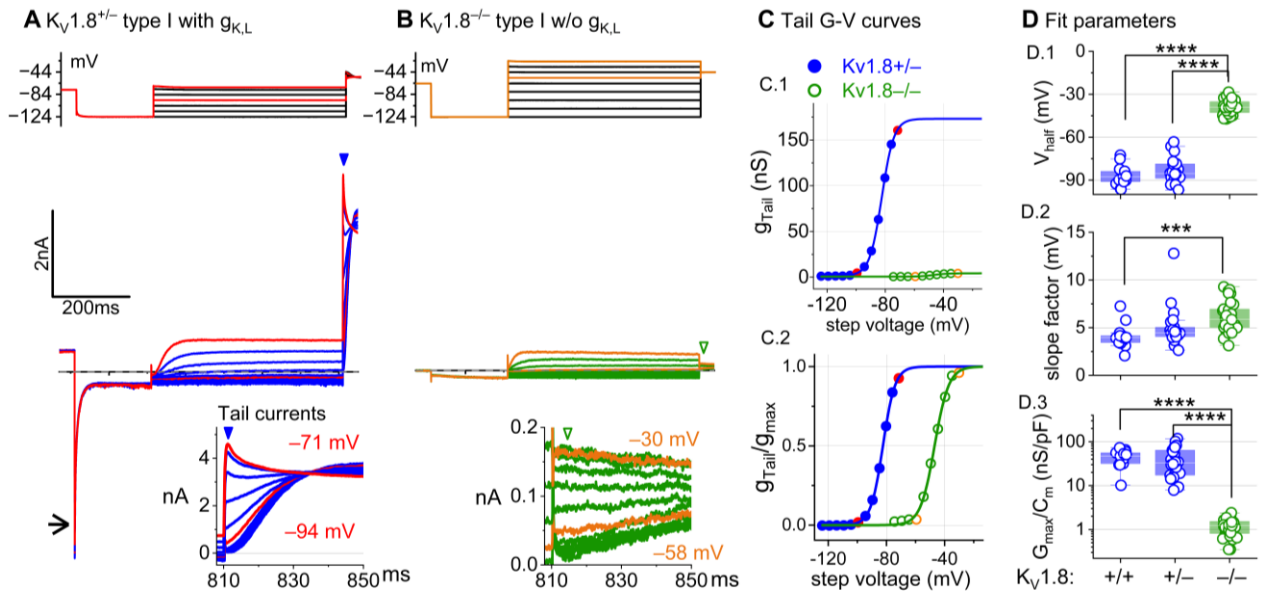

Figure 1. $K_V1.8^{-/-}$ type I hair cells lacked $g_{K,L}$, the dominant conductance in mature $K_V1.8^{+/+,+/-}$ type I HCs. Representative voltage-evoked currents in **(A)** a P22 $K_V1.8^{+/-}$ type I HC and **(B)** a P29 $K_V1.8^{-/-}$ type I HC. (A) *Arrow,* transient inward current that is a hallmark of $g_{K,L}$. *Arrowheads,* tail currents, magnified in *insets*. For steps positive to the midpoint voltage, tail currents are very large. As a result, K^+ accumulation in the calyceal cleft reduces driving force on K^+, causing currents to decay rapidly, as seen in A (Lim et al., 2011). Note that the voltage protocol (top) in B extends to more positive voltages. **(C)** Activation (G-V) curves from tail currents in A and B; symbols, data; curves, Boltzmann fits (Eq. 1). **(D)** Fit parameters from mice >P12 show big effect of $K_V1.8^{-/-}$ and no difference between $K_V1.8^{+/-}$ and $K_V1.8^{+/+}$. *Asterisks* (here and elsewhere): *, p<0.05; **, p<0.01; ***, p<0.001; and ****, p<0.0001. *Line,* median; *Box,* interquartile range; *Whiskers*, outliers. See Table 1 for statistics.

seen in the delayed rectifier currents of immature type I HCs (Suppl. Fig. 1B), showing that they were not immature forms of the $K_V1.8$-dependent $g_{K,L}$ channels.

$K_V1.8^{-/-}$ type I HCs had a much smaller residual delayed rectifier that activated positive to resting potential, with V_{half} ~–40 mV and g_{max} density of 1.3 nS/pF. No additional K^+ conductance activated up to +40 mV, and G-V parameters did not change much with age from P5 to P370. We characterize this $K_V1.8$-independent delayed rectifier later. A much larger non-$g_{K,L}$ delayed rectifier conductance ("$g_{DR,I}$") was reported in our earlier publication on mouse utricular type I HCs (Rüsch et al., 1998). This current was identified as that remaining after "blocking" $g_{K,L}$ with 20 mM external Ba^{2+}. Our new data suggest that there is no large non-$g_{K,L}$ conductance, and that instead high Ba^{2+} positively shifted the apparent voltage dependence of $g_{K,L}$.

$K_V1.8$ strongly affects type I passive properties and responses to current steps.

While the cells of $K_V1.8^{-/-}$ and $K_V1.8^{+/-}$ epithelia appeared healthy, type I hair cells had smaller membrane capacitances (C_m): 4-5 pF in $K_V1.8^{-/-}$ type I HCs, ~20% smaller than $K_V1.8^{+/-}$ type I HCs (~6 pF) and ~30% smaller than $K_V1.8^{+/+}$ type I HCs (6-7 pF; Table 2). C_m scales with surface area, but soma sizes were unchanged by deletion of $K_V1.8$ (Suppl. Table 2). Instead, C_m may be higher in $K_V1.8^{+/+}$ cells because of $g_{K,L}$ for two reasons. First, highly expressed trans-membrane proteins (see discussion of $g_{K,L}$ channel density in Chen and Eatock, 2000) can affect membrane thickness (Mitra et al., 2004), which is inversely proportional to specific C_m. Second, $g_{K,L}$ could contaminate estimations of capacitive current, which is

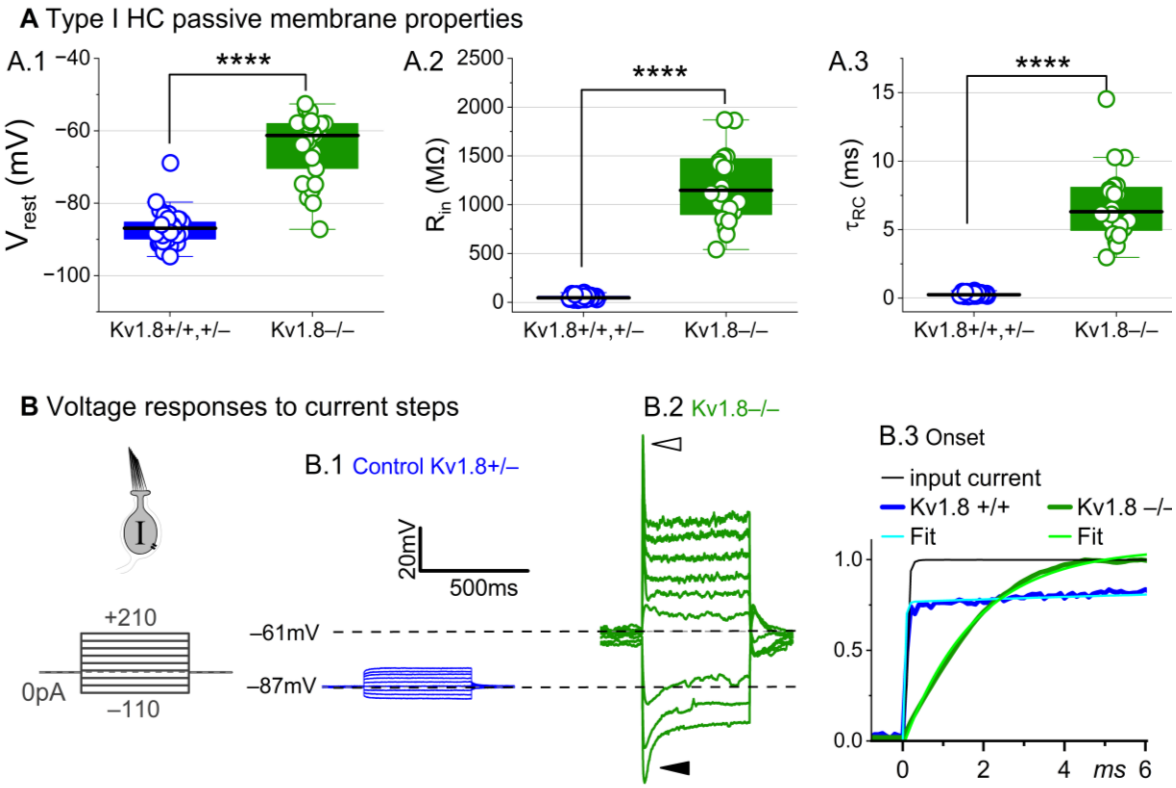

Figure 2. $K_V1.8^{-/-}$ type I hair cells had much longer membrane charging times and higher input resistances (voltage gains) than $K_V1.8^{+/+,+/-}$ type I HCs. (A) $g_{K,L}$ strongly affects passive membrane properties: (**A.1**) V_{rest} , (**A.2**) R_{in}, input resistance, and (**A.3**) membrane time constant, τ_{RC} = (R_{input} * C_m). See Table 2 for statistics. **(B)** Current clamp responses to the same scale from (B.1) $K_V1.8^{+/-}$ and (B.2) $K_V1.8^{-/-}$ type I cells, both P29. *Filled arrowhead (B.2),* sag indicating I_H activation. *Open arrowhead*, Depolarization rapidly decays as I_{DR} activates. B.3, The 1st 6 ms of voltage responses to 170-pA injection is normalized to steady-state value; overlaid curves are double-exponential fits ($K_V1.8^{+/+}$, τ 40 µs and 2.4 ms) and single-exponential fits ($K_V1.8^{-/-}$, τ 1.1 ms) .

calculated from the decay time constant of transient current evoked by a small voltage step *outside* the operating range of any ion channels. $g_{K,L}$ has such a negative operating range that, even for V_m negative to –90 mV, some $g_{K,L}$ channels are voltage-sensitive and could add to capacitive current.

Basolateral conductances help set the resting potential and passive membrane properties that regulate the time course and gain of voltage responses to small currents. To examine the effect of $K_V1.8$ on these properties, we switched to current clamp mode and measured resting potential (V_{rest}), input resistance (R_{in}, equivalent to voltage gain for small current steps, △V/△I), and membrane time constant (τ_{RC}). In $K_V1.8^{-/-}$ type I HCs, V_{rest} was much less negative (Fig. 2A.1), R_{in} was greater by ~20-fold (Fig. 2A.2), and membrane charging times were commensurately longer (Fig. 2A.3).

The differences between the voltage responses of $K_V1.8^{+/+,+/-}$ and $K_V1.8^{-/-}$ type I HCs are expected from the known impact of $g_{K,L}$ on V_{rest} and R_{in} (Correia and Lang, 1990; Ricci et al., 1996; Rüsch and Eatock, 1996b; Songer and Eatock, 2013). The large K^+-selective conductance at V_{rest} holds V_{rest} close to E_K (K^+ equilibrium potential) and minimizes gain (△V/△I), such that voltage-gated conductances are negligibly affected by the input current and the cell produces approximately linear, static responses to iterated current steps. For $K_V1.8^{-/-}$ type I HCs, with their less negative V_{rest} and larger R_{in}, positive current steps evoked a fast initial depolarization (Fig. 2B.2), activating residual delayed rectifiers and repolarizing the

Table 1. *Type I hair cell K_V activation voltage dependence and kinetics. Mean ± SEM (number of cells). g is effect size, Hedge's g. KWA is Kruskal-Wallis ANOVA.*

Zone	$K_V1.8$	Tail $V_{1/2}$, mV [a]	Tail S, mV [b]	Tail G_{max}, nS [c]	Tail G_{max}/C_m, nS/pF [d]	Age (median, range)
Extrastriola	+/+	–85 ± 2 (12)	4.3 ± 0.4 (12)	270 ± 40 (11)	47 ± 8 (11)	22, 14-287
	+/–	–83 ± 1 (40)	5.2 ± 0.3 (40)	210 ± 20 (40)	37 ± 4 (40)	19, 13-259
	–/–	–40.2 ± 0.9 (26)	5.7 ± 0.3 (26)	5.4 ± 0.3 (26)	1.11 ± 0.08 (26)	45, 14-277
Striola	+/+	–87 ± 3 (6)	4.3 ± 0.3 (6)	310 ± 70 (6)	41 ± 7 (6)	40, 15-59
	+/–	–88 ± 2 (3)	4.7 ± 0.9 (3)	270 ± 60 (3)	44 ± 6 (3)	19, 14-20
	–/–	–38 ± 1 (13)	6.2 ± 0.4 (13)	6.5 ± 0.6 (13)	1.5 ± 0.1 (13)	202, 14-370

[a] –/– vs +/+: 2-way ANOVA, p < 1E-9, g 7.7; –/– vs +/–: 2-way ANOVA, p < 1E-9, g 6.8
[b] –/– vs +/+: 2-way ANOVA, p = 8.4E-4, g 1.2
[c] –/– vs +/+: 2-way ANOVA, p < 1E-9, g 3.7; –/– vs +/–: 2-way ANOVA, p < 1E-9, g 2.1
[d] –/– vs +/+: 2-way ANOVA, p < 1E-9, g 3.6; –/– vs +/–: 2-way ANOVA, p < 1E-9, g 2.0

Table 2. *Type I hair cell* p*assive membrane properties. Mean ± SEM (number of cells). g is effect size, Hedge's g. KWA is Kruskal-Wallis ANOVA.*

Zone	*$K_V1.8$*	*V_{rest}, mV* [a, b]	R_{input}, MΩ [c]	τ_{RC}, ms [d]	C_m (pF) [e]	Age (median, range)
Extrastriola	+/+	–84 ± 3 (6)	44 ± 6 (6)	0.24 ± 0.03 (6)	6.1 ± 0.4 (13)	19.5, 14-287
	+/–	–88.0 ± 0.7 (28)	55 ± 5 (24)	0.32 ± 0.03 (23)	5.8 ± 0.2 (44)	21, 16-29
	–/–	–63 ± 2 (15)	1400 ± 100 (15)	6.4 ± 0.6 (15)	5 ± 0.2 (27)	45, 14-202
Striola	+/+	–87 ± 2 (4)	50 ± 8 (4)	0.30 ± 0.04 (4)	7.4 ± 0.7 (7)	43, 40-59
	+/–	–87 ± 3 (3)	38 ± 8 (2)	0.21 ± 0.01 (2)	5.9 ± 0.6 (3)	19, 19-20
	–/–	–74 ± 5 (5)	1000 ± 300 (4)	4.2 ± 1.0 (4)	4.4 ± 0.2 (14)	202, 24-370

[a] striolar –/– vs ES –/–: 2-way ANOVA, p = 0.006, g 1.2; striolar –/– vs striolar +/+,+/–: 2-way ANOVA, p = 0.005, g 1.7
[b] –/– vs +/+: 2-way ANOVA, p < 1E-9, g 2.3; –/– vs +/–: 2-way ANOVA, p < 1E-9, g 3.4
[c] –/– vs +/+: 2-way ANOVA, p < 1E-9, g 3.1; –/– vs +/–: 2-way ANOVA, p < 1E-9, g 3.9
[d] –/– vs +/+: 2-way ANOVA, p < 1E-9, g 2.7; –/– vs +/–: 2-way ANOVA, p < 1E-9, g 3.4
[e] –/– vs +/+: 2-way ANOVA, p = 3E-7, g 1.5; –/– vs +/–: 2-way ANOVA, p = 1.3E-4, g 1.0; +/– vs +/+: 2-way ANOVA, p = 0.048, g 0.6

membrane toward E_K. Negative current steps evoked an initial "sag" (Fig. 2B.2), a hyperpolarization followed by slow repolarization as the HCN1 channels open (Rüsch and Eatock, 1996b; Horwitz et al., 2011).

Overall, comparison of the $K_V1.8^{+/+,+/-}$ and $K_V1.8^{-/-}$ responses shows that with $K_V1.8$ ($g_{K,L}$), the voltage response of the type I hair cell is smaller but better reproduces the time course of the input current.

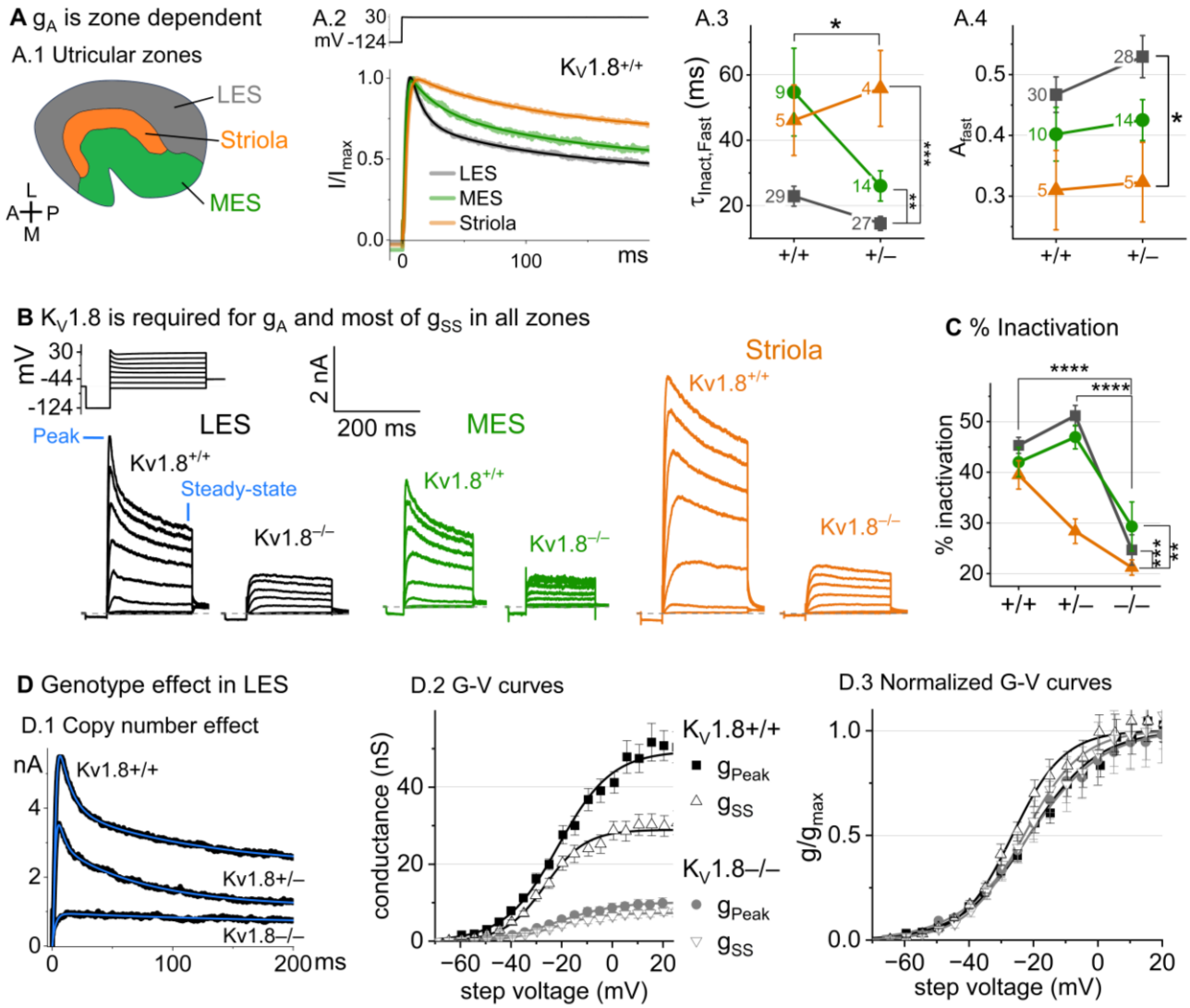

Figure 3. $K_V1.8^{-/-}$ type II HCs in all zones of the sensory epithelium lacked the major rapidly inactivating conductance, g_A, and had less delayed rectifier conductance. Activation and inactivation varied with epithelial zone and genotype. (**A**) g_A inactivation time course varied across zones. (**A.1**) Zones of the utricular epithelium. (**A.2**) Normalized currents evoked by steps from –124 mV to +30 mV with overlaid fits of Eq. 3. (**A.3**) $\tau_{Inact,Fast}$ was faster in $K_V1.8^{+/-}$ than $K_V1.8^{+/+}$ HCs , and faster in LES than other zones. Brackets show post hoc pairwise comparisons between two zones (vertical brackets) and horizontal brackets compare two genotypes; see Table 3 for statistics. (**A.4**) Fast inactivation was a greater fraction of total inactivation in LES than striola.
(**B**) Exemplars; ages, *left to right*, P312, P53, P287, P49, P40, P154.
(**C**) % inactivation at 30 mV was much lower in $K_V1.8^{-/-}$ than $K_V1.8^{+/-}$ and $K_V1.8^{+/+}$, and lower in striola than LES and MES. Interaction between zone and genotype was significant (Table 3).
(**D**) Exemplar currents and G-V curves from LES type II HCs show a copy number effect. (**D.1**) Currents for examples of the 3 genotypes evoked by steps from –124 mV to +30 mV fit with Eq. 3. (**D.2**) Averaged peak and steady-state conductance-voltage datapoints from LES cells (+/+, n=37; –/–, n=20) were fit with Boltzmann equations (Eq. 1) and normalized by g_{max} in (**D.3**). See Table 4 for statistics.

$K_V1.8$ is necessary for both inactivating and non-inactivating K_V currents in type II hair cells

Type II HCs also express $K_V1.8$ mRNA (McInturff et al., 2018; Orvis et al., 2021). Although their outwardly-rectifying conductances (g_A and g_{DR}) differ substantially in voltage dependence and size from $g_{K,L}$, both conductances were strongly affected by the null mutation: g_A was eliminated and the delayed rectifier

was substantially smaller. Below we describe g_A and g_{DR} in $K_V1.8^{+/+,+/-}$ type II HCs and the residual outward rectifying current in $K_V1.8^{-/-}$ type II HCs.

$K_V1.8^{+/+,+/-}$ type II HCs. Most (81/84) $K_V1.8^{+/+,+/-}$ type II HCs expressed a rapidly-activating, rapidly-inactivating A-type conductance (g_A). We define A current as the outwardly rectifying current that inactivates by over 30% within 200 ms. g_A was more prominent in extrastriolar zones, as reported (Holt et al. 1999, Weng and Correia 1999).

We compared the activation and inactivation time course and inactivation prominence for 200-ms steps from –124 mV to ~30 mV. Outward currents fit with Eq. 3 yielded fast inactivation time constants ($\tau_{Inact, Fast}$) of ~30 ms in LES (Fig. 3A.2). $\tau_{Inact, Fast}$ was faster in LES than in MES or striola (Fig. 3A.3) and fast inactivation was a larger fraction of the total inactivation in LES than striola (~0.5 vs. 0.3, Fig. 3A.4).

To show voltage dependence of activation, we generated G-V curves for peak currents (sum of A-current and delayed rectifier) and steady-state currents measured at 200 ms, after g_A has mostly inactivated (Figure 3D.2). $K_V1.8^{+/-}$ HCs had smaller currents than $K_V1.8^{+/+}$ HCs, reflecting a smaller g_{DR} (Fig. 3D) and faster fast inactivation (Fig. 3A.3). As discussed later, these effects may relate to effects of the $K_V1.8$ gene dosage on the relative numbers of different $K_V1.8$ heteromers.

For $K_V1.8^{+/+}$ and $K_V1.8^{+/-}$ HCs, the voltage dependence as summarized by V_{half} and slope factor (S) was similar. Relative to g_{SS}, g_{Peak} had a more positive V_{half} (~–21 vs. ~–26) and greater S (~12 vs. ~9, Fig. 3D, Table 4). Because g_{Peak} includes channels with and without fast inactivation, the shallower g_{Peak}-V curve may reflect a more heterogeneous channel population. Only g_{Peak} showed zonal variation, with more positive V_{half} in LES than striola (~–20 mV vs. ~–24 mV, Fig. 3D, Table 4). We later suggest that variable subunit composition may drive zonal variation in g_{Peak}.

$K_V1.8^{-/-}$ type II HCs from all zones were missing g_A and 30-50% of g_{DR} (Fig. 3B-D). The residual delayed rectifier (1.3 nS/pF) had a more positive V_{half} than g_{DR} in $K_V1.8^{+/+,+/-}$ HCs (~–20 mV *vs.* ~–26 mV, Fig. 3D.2). We refer to the $K_V1.8$-dependent delayed rectifier component as $g_{DR}(K_V1.8)$ and to the residual, $K_V1.8$-*in*dependent delayed rectifier component as $g_{DR}(K_V7)$ because, as we show later, it includes K_V7 channels.

Supplemental Figure 3A shows the development of $K_V1.8$-dependent and independent K_V currents in type II HCs with age from P5 to over P300. In $K_V1.8^{+/+,+/-}$ type II HCs, g_A was present at all ages with a higher % inactivation after P18 than at P5-P10 (Suppl. Fig. 3A.4). g_{Peak} did not change much above P12 except for a compression of conductance density from P13 to P370 (partial correlation coefficient = –0.4, p = 2E-5, Suppl. Fig. 3A.3).

We saw small rapidly inactivating outward currents in a minority of $K_V1.8^{-/-}$ type II HCs (23%, 7/30), all >P12 and extrastriolar (Suppl. Fig. 4). These currents overlapped with g_A in percent inactivation, inactivation kinetics, and activation voltage dependence but were very small. As discussed later, we suspect that these currents flow through homomers of inactivating K_V subunits that in control hair cells join with $K_V1.8$ subunits and confer inactivation on the heteromeric conductance.

$K_V1.8$ affects type II passive properties and responses to current steps.

In type II HCs, absence of $K_V1.8$ did not change V_{rest} (Fig. 4A.1) because g_A and g_{DR} both activate positive to rest, but significantly increased R_{in} and τ_{RC} (Fig. 4A.2-A.3).

Table 3. *Type II hair cell K_V currents: Activation and inactivation time course at +30 mV. Mean ± SEM. g is effect size, Hedge's g. KWA is Kruskal-Wallis ANOVA.*

Zone	$K_V1.8$	τ_{Act} at 30 mV, ms [a, b]	$\tau_{Inact,Fast}$ at 30 mV, ms [c, d]	Fast inactivation prominence [e]	Inactivation % [f, g]	N cells	Age (median, range)
LES	+/+	2.11 ± 0.09	23 ± 3	0.46 ± 0.03	45 ± 2	30	46, 14-312
	+/–	1.64 ± 0.09	15 ± 2	0.53 ± 0.03	51 ± 2	27	29, 13-280
	–/–	4.4 ± 0.5	*NA*	*NA*	25 ± 3	21	128, 15-355
MES	+/+	2.8 ± 0.5	50 ± 10	0.40 ± 0.04	42 ± 3	9	94, 22-296
	+/–	2.2 ± 0.2	90 ± 60	0.42 ± 0.03	47 ± 2	15	24, 13-52
	–/–	10 ± 7	*NA*	*NA*	29 ± 5	10	84, 28-355
Striola	+/+	2.7 ± 0.3	50 ± 10	0.31 ± 0.07	39 ± 3	5	45, 40-287
	+/–	2.9 ± 0.4	300 ± 200	0.3 ± 0.06	28 ± 2	5	19, 14-30
	–/–	7 ± 2	*NA*	*NA*	22 ± 2	6	202, 29-298

[a] –/– vs +/+: KWA, p = 0.0048, g 0.6; –/– vs +/–: KWA, p = 2.3E-7, g 0.6
[b] Striola vs LES: KWA, p = 5.7E-4, g 1.0
[c] +/– vs +/+: KWA, p = 0.027, g 0.2
[d] LES vs MES: KWA, p = 0.0018, g 0.3; LES vs Striola: KWA, p = 1.9E-4, g 0.8
[e] LES vs Striola: 2-way ANOVA, p = 0.0041, g 0.7
[f] –/– vs +/+: 2-way ANOVA, p < 1E-9, g 1.7; –/– vs +/–: 2-way ANOVA, p < 1E-9, g 1.8
[g] Striola vs LES: 2-way ANOVA, p = 3.4E-5, g 0.9; Striola vs MES: 2-way ANOVA, p = 0.0011, g 1.0; Interaction between genotype and Zone: 2-way ANOVA, p = 0.026

Table 4. *Type II hair cell K_V currents: Activation voltage dependence. Mean ± SEM. g is effect size, Hedge's g. KWA is Kruskal-Wallis ANOVA.*

Zone	*$K_V1.8$*	*Peak $V_{1/2}$, mV* [a]	Peak S, mV [b, c]	A-type g_{max}/C_m, nS/pF [d]	SS V_{half}, mV [e]	SS S, mV [f]	SS g_{max}/C_m, nS/pF [g, h]	N cells	Age (median, range)
LES	+/+	–19.8 ± 0.6	11.8 ± 0.4	4.0 ± 0.3	–25.0 ± 0.5	8.7 ± 0.3	7.1 ± 0.8	37	46, 14-312
	+/–	–19.8 ± 0.8	12.8 ± 0.4	3.8 ± 0.3	–26.8 ± 0.8	8.7 ± 0.3	4.9 ± 0.4	35	29, 13-280
	–/–	–18 ± 1	11.7 ± 0.4	0.37 ± 0.05	–19 ± 1	12.1 ± 0.5	1.8 ± 0.2	20	128, 15-355
MES	+/+	–22 ± 1	11 ± 0.7	4.1 ± 0.7	–26 ± 1	8.3 ± 0.5	9 ± 1	11	94, 22-296
	+/–	–21 ± 1	11.8 ± 0.4	3.6 ± 0.5	–27 ± 1	9.0 ± 0.3	5.9 ± 0.7	16	24, 13-52
	–/–	–19 ± 1	10.8 ± 0.6	0.6 ± 0.1	–20 ± 1	10.7 ± 0.7	2.5 ± 0.3	15	84, 28-355
Striola	+/+	–24 ± 1	9.6 ± 0.5	5 ± 1	–26.6 ± 0.9	8.2 ± 0.4	12 ± 1	7	45, 40-287
	+/–	–25 ± 2	9.4 ± 0.4	2.6 ± 0.6	–28 ± 2	8.2 ± 0.3	10 ± 2	6	19, 14-30
	–/–	–21.3 ± 0.9	10.3 ± 0.5	0.7 ± 0.1	–21.7 ± 0.8	10.5 ± 0.6	3.9 ± 0.5	8	202, 29-298

[a] Striola vs LES: 2-way ANOVA, p = 0.00116, g 0.9
[b] Striola vs MES: 2-way ANOVA, p = 0.016, g 0.8; Striola vs LES: 2-way ANOVA, p = 7.5E-6, g 1.2
[c] –/– vs +/–: 2-way ANOVA, p = 0.036, g 0.5
[d] –/– vs +/+: Welch ANOVA, p < 1E-9, g 2.3; –/– vs +/–: Welch ANOVA, p < 1E-9, g 2.3
[e] –/– vs +/+: 2-way ANOVA, p < 1E-9, g 1.4; –/– vs +/–: 2-way ANOVA, p < 1E-9, g 1.6
[f] –/– vs +/+: 2-way ANOVA, p < 1E-9, g 1.4; –/– vs +/–: 2-way ANOVA, p = 4.5E-7, g 1.1
[g] –/– vs +/+: Welch ANOVA, p < 1E-9, g 1.6; –/– vs +/–: Welch ANOVA, p < 1E-9, g 1.3; +/+ vs +/–: Welch ANOVA, p = 0.007, g 1.6
[h] Striola vs LES: 1-way ANOVA, p = 0.001, g 0.9); Striola vs MES: 1-way ANOVA, p = 0.01, g 0.8

Positive current steps evoked an initial depolarizing transient in both $K_V1.8^{+/+}$ and $K_V1.8^{-/-}$ type II HCs, but the detailed time course differed (Fig. 4B). Both transient and steady-state responses were larger in

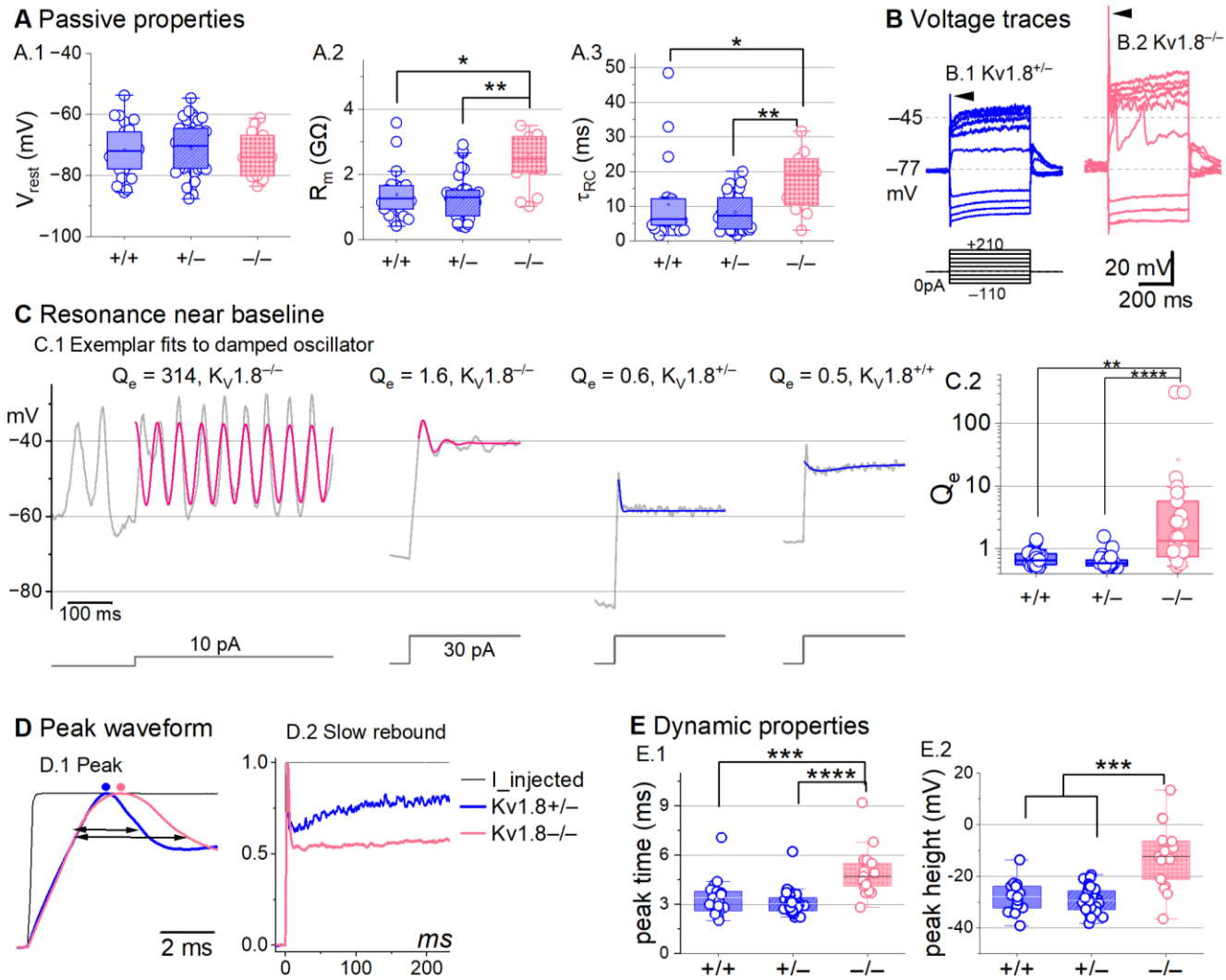

Figure 4. $K_V1.8^{-/-}$ type II hair cells had larger, slower voltage responses and more electrical resonance. **(A)** Passive membrane properties near resting membrane potential: A.1) Resting potential. R_{input} (A.2) and τ_{RC} (A.3) were obtained from single exponential fits to voltage responses < 15 mV. See Table 5 for statistics.
(**B**) Exemplar voltage responses to iterated current steps (*bottom)* illustrate key changes in gain and resonance with $K_V1.8$ knockout. (**B.1**) $K_V1.8^{+/-}$ type II HC (P24, LES) and (**B.2**) $K_V1.8^{-/-}$ type II HC (P53, LES). *Arrowheads,* depolarizing transients.
(**C**) Range of resonance illustrated for $K_V1.8^{-/-}$ type II HCs (*left, pink curves fit to Eq. 5*) and controls (*right, blue fits*). (**C.1**) *Resonant frequencies, left to right:* 19.6, 18.4, 34.4, 0.3 Hz. Leftmost cell resonated spontaneously (before step). (**C.2**) Tuning quality (Q_e; Eq. 6) was higher for $K_V1.8^{-/-}$ type II HCs (KWA, p = 0.0064 vs. $K_V1.8^{+/+}$; p = 7E-8 vs. $K_V1.8^{+/-}$).
(**D**) $K_V1.8^{-/-}$ type II HCs had higher, slower peaks and much slower rebound potentials in response to large (170-pA) current steps. (**D.1**) Normalized to show initial depolarizing transient (*filled circles*, times of peaks; *horizontal arrows*, peak width at half-maximum). (**D.2**) Longer time scale to highlight how null mutation reduced post-transient rebound.
(**E**) In $K_V1.8^{-/-}$ HCs, depolarizing transients evoked by a +90-pA step were slower to peak (**E.1**) and (**E.2**) larger.

$K_V1.8^{-/-}$, consistent with their larger R_{in} values.

Absence of $K_V1.8$ increased the incidence of sharp electrical resonance in type II HCs. Electrical resonance, which manifests as ringing responses to current steps, can support receptor potential tuning (Ashmore, 1983; Fettiplace, 1987; Hudspeth and Lewis, 1988; Ramanathan and Fuchs, 2002). Larger R_{in} values made $K_V1.8^{-/-}$ type II HCs more prone to electrical resonance; Figure 4C.1 shows a striking example.

Table 5. *Type II hair cell passive membrane properties. Mean ± SEM (number of cells). g is effect size, Hedge's g. KWA is Kruskal-Wallis ANOVA.*

Zone	$K_V1.8$	V_{rest}, mV	R_{input}, GΩ [a]	τ_{RC}, ms [b]	Peak height, mV, 170 [c]	Peak time, ms [d]	C_m, pF	Age (median, range)
Extrastriola	+/+	–71 ± 2 (19)	1.4 ± 0.2 (16)	11 ± 3 (16)	–20 ± 2 (15)	2.5 ± 0.2 (15)	4.7 ± 0.2 (50)	45, 16-312
	+/–	–71 ± 2 (34)	1.2 ± 0.1 (27)	9 ± 1 (27)	–20 ± 1 (30)	2.44 ± 0.08 (30)	4.6 ± 0.1 (52)	27, 13-280
	–/–	–76 ± 2 (9)	2.3 ± 0.3 (7)	16 ± 3 (7)	2 ± 6 (7)	3.6 ± 0.3 (7)	4.6 ± 0.2 (35)	53, 15-154
Striola	+/+	–73.1 ± 1.0 (6)	1.4 ± 0.1 (6)	9 ± 1 (6)	–20 ± 2 (5)	2.7 ± 0.1 (5)	4.6 ± 0.2 (7)	45, 40-224
	+/–	–71 ± 3 (5)	1.4 ± 0.3 (6)	7 ± 2 (6)	–20 ± 2 (6)	2.3 ± 0.1 (6)	4.8 ± 0.2 (6)	19, 19-30
	–/–	–68 ± 2 (6)	3.0 ± 0.7 (6)	26 ± 10 (6)	2 ± 7 (4)	4 ± 1 (4)	4.4 ± 0.3 (7)	178, 29-298

[a] –/– vs +/+: KWA, p = 0.015, g 1.2; –/– vs +/–: KWA, p = 0.002, g 1.5
[b] –/– vs +/+: KWA, p = 0.016, g 0.7; –/– vs +/–: KWA, p = 0.008, g 1.2
[c] –/– vs +/+: KWA, p = 0.006, g 2.1; –/– vs +/–: KWA, p = 2E-4, g 2.6
[d] –/– vs +/+: 2-way ANOVA, p <1E-9, g 1.3; –/– vs +/–: 2-way ANOVA, p < 1E-9, g 1.9

Median resonance quality (Q_e, sharpness of tuning) was greater in $K_V1.8^{-/-}$ (1.33, n=26) than $K_V1.8^{+/+}$ (0.66, n=23) or $K_V1.8^{+/-}$ (0.59, n=44) type II HCs.

$K_V1.8$ affected the time course of the initial peak in response to much larger current injections (Fig. 4D-E). Fast activation of g_A in control type II HCs rapidly repolarizes the membrane and then inactivates, allowing the constant input current to progressively depolarize the cell, producing a slow rebound (Fig 4D.2). This behavior has the potential to counter mechanotranduction adaptation (Vollrath and Eatock, 2003).

$K_V1.8$ immunolocalized to basolateral membranes of both type I and II HCs

If $K_V1.8$ is a pore-forming subunit in the $K_V1.8$-dependent conductances $g_{K,L}$, g_A, and g_{DR}, it should localize to hair cell membranes. Figure 5 compares $K_V1.8$ immunoreactivity in $K_V1.8^{+/+}$ and $K_V1.8^{-/-}$ utricles, showing specific immunoreactivity along the basolateral membranes of both hair cell types in $K_V1.8^{+/+}$ utricles. To identify hair cell type and localize the hair cell membrane, we used antibodies against $K_V7.4$ (KCNQ4), an ion channel densely expressed in the calyceal "inner-face" membrane next to the synaptic cleft (Hurley et al., 2006; Lysakowski et al., 2011), producing a cup-like stain around type I HCs (Fig. 5A). $K_V1.8$ immunoreactivity was present in hair cell membrane apposing $K_V7.4$-stained calyx inner face in $K_V1.8^{+/+}$ utricles (Fig. 5A.1, A.2) and not in $K_V1.8^{-/-}$ utricles (Fig. 5A.3).

In other experiments, we used antibodies against calretinin (Calb2), a cytosolic calcium binding protein expressed by many type II HCs and also by striolar calyx-only afferents (Desai et al., 2005; Lysakowski et al., 2011) (Fig. 5B). A hair cell is type II if it is calretinin-positive (Fig. 5B.1) or if it lacks a $K_V7.4$-positive or

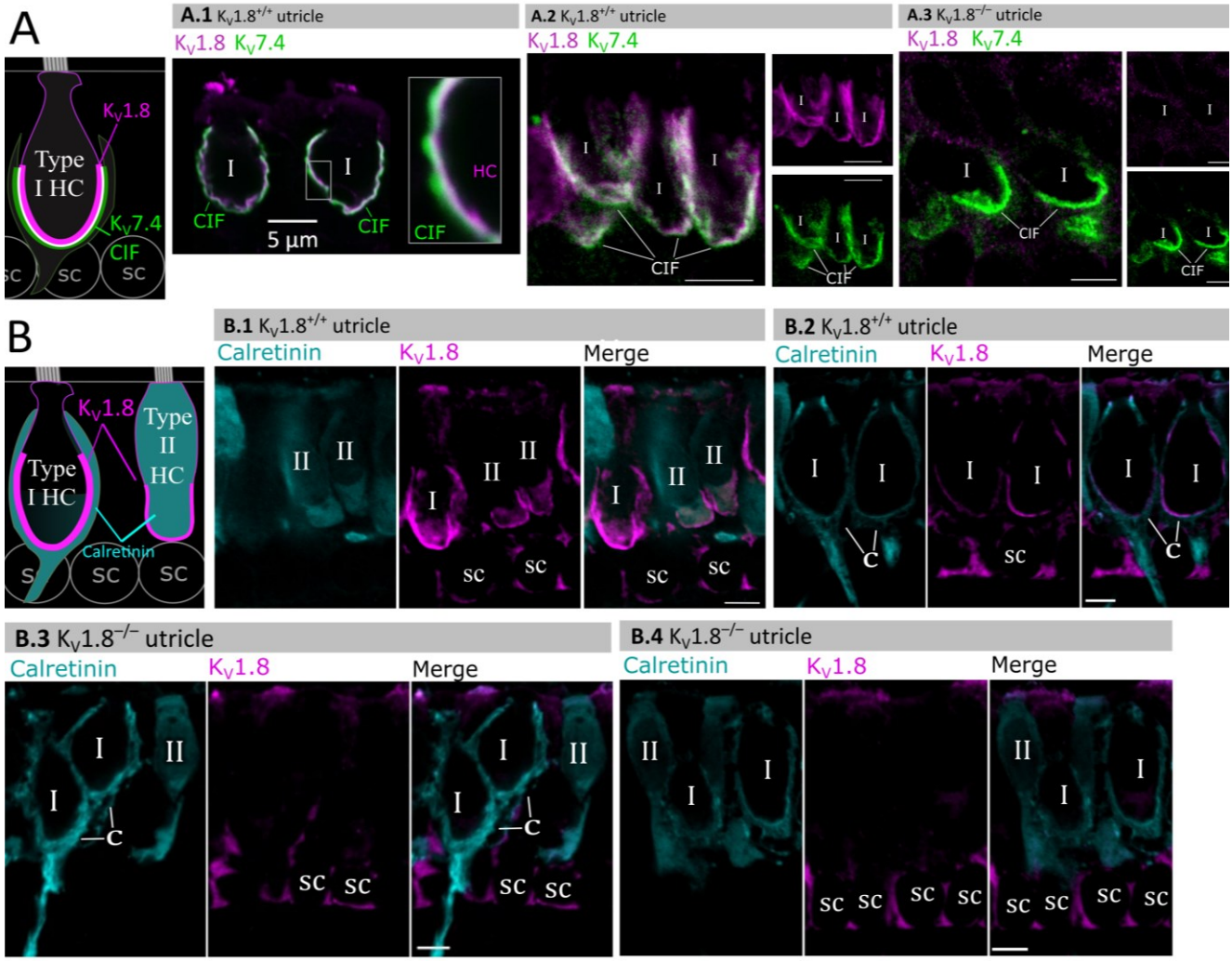

Figure 5. **Type I and type II HC basolateral membranes show specific immunoreactivity to Kv1.8 antibody (magenta).** Antibodies for $K_V7.4$ (A, green) and calretinin (B, cyan) were used as counterstains for calyx membrane (Kv7.4), type II HC cytoplasm (calretinin) and cytoplasm of striolar calyx-only afferents (calretinin). (**A**) *Left,* Cartoon showing $K_V7.4$ on the calyx inner face membrane (CIF) and $K_V1.8$ on the type I HC membrane. SC, supporting cell nuclei. *A.1-3*, Adult mouse utricle sections. $K_V7.4$ antibody labeled calyces on two $K_V1.8$-positive type I HCs (**A.1**), four $K_V1.8$-positive type I HCs (**A.2**), and two $K_V1.8$-negative type I HCs from a $K_V1.8^{-/-}$ mouse (**A.3**). (**B**) *Left,* Cartoon showing cytoplasmic calretinin stain in calyx-only striolar afferents and most type II HCs, and $K_V1.8$ on membranes of both HC types. In wildtype utricles, $K_V1.8$ immunolocalized to basolateral membranes of type I and II HCs (**B.1**). $K_V1.8$ immunolocalized to type I HCs in striola (**B.2**). Staining of supporting cell (SC) membranes by Kv1.8 antibody was non-specific, as it was present in $K_V1.8^{-/-}$ tissue (**B.3, B.4**).

258 calretinin-positive calyceal cup (Fig. 5A.2, 5B.3, rightmost cells). Hair cell identification was confirmed with
259 established morphological indicators: for example, type II HCs tend to have basolateral processes (feet)
260 (Pujol et al., 2014) and, in the extrastriola, more apical nuclei than type I HC.

261 Previously, Carlisle et al. (2012) reported $K_V1.8$-like immunoreactivity in many cell types in the inner
262 ear. In contrast, Lee et al. (2013) found that gene expression reporters indicated expression only in hair
263 cells and some supporting cells. Here, comparison of control and null tissue showed selective expression
264 of HC membranes, and that some supporting cell staining is non-specific.
265

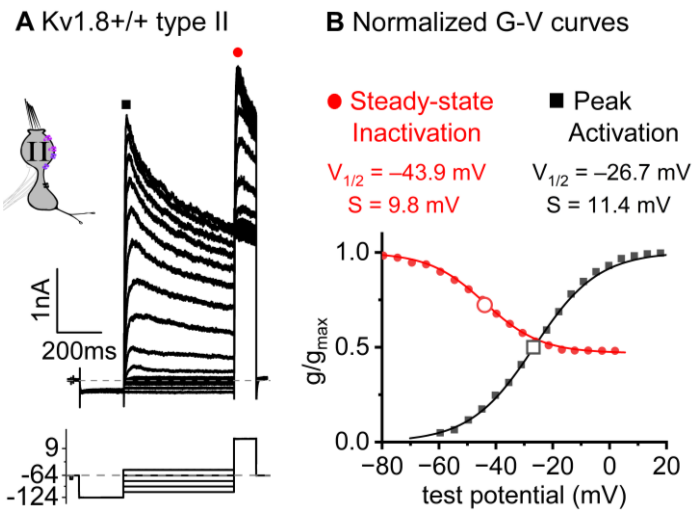

Figure 6. Inactivation curve of g_A in extrastriolar type II HCs.
(**A**) Modified voltage protocol measured accumulated steady-state inactivation in the tail potential. 100 µM ZD7288 in bath prevented contamination by HCN current. (**B**) Voltage dependence of g_A's steady-state inactivation (h_∞ curve) and peak activation are consistent with $K_V1.4$ heteromers. H_∞ curves have overlapped normalized activation (peak conductance, black squares) and inactivation (tail conductance, red circles) G-V data points. *Curves,* Boltzmann fits (Eq. 1). *Average fit parameters* from $K_V1.8^{+/+,+/-}$ type II HCs, P40-P210, median P94. Inactivation: V_{half}, –42 ±2 mV (n=11); S, 11 ± 1 mV. Activation: V_{half}, –23 ± 1 mV (n=11); S, 11.2 ± 0.4 mV.

$K_V1.4$ may also contribute to g_A

Results with the $K_V1.8$ knockout suggest that type II hair cells have an inactivating K_V1 conductance that includes $K_V1.8$ subunits. $K_V1.8$, like most K_V1 subunits, does not show fast inactivation as a heterologously expressed homomer (Lang et al., 2000; Ranjan et al., 2019; Dierich et al., 2020), nor do the $K_V1.8$-dependent channels in type I HCs, as we show, and in cochlear inner hair cells (Dierich et al., 2020). K_V1 subunits without intrinsic inactivation can produce rapidly inactivating currents by associating with $K_V\beta1$ (KCNB1) or $K_V\beta3$ subunits. $K_V\beta1$ is present in type II HCs alongside $K_V\beta2$ (McInturff et al., 2018; Jan et al., 2021; Orvis et al., 2021), which does not confer rapid inactivation (Dwenger et al., 2022).

Another possibility is that in type II HCs, $K_V1.8$ subunits heteromultimerize with $K_V1.4$ subunits—the only K_V1 subunits which, when expressed as a homomer, have complete N-type (fast) inactivation (Stühmer et al., 1989). Multiple observations support this possibility. $K_V1.4$ has been linked to g_A in pigeon type II HCs (Correia et al., 2008) and is the second-most abundant K_V1 transcript in mammalian vestibular HCs, after $K_V1.8$ (Scheffer et al., 2015). $K_V1.4$ is expressed in type II HCs but not type I HCs (McInturff et al., 2018; Orvis et al., 2021), and is not found in striolar HCs (Jan et al., 2021; Orvis et al., 2021), where even in type II HCs, inactivation is slower and less extensive (Fig. 3A).

Functional heteromers form between $K_V1.4$ and other $K_V1.x$ and/or $K_V\beta1$ (Imbrici et al., 2006; Correia et al., 2008; Al-Sabi et al., 2011). Although $K_V1.4$ and $K_V1.8$ heteromers have not been studied directly, g_A's inactivation time course ($\tau_{Fast,Inac}$ of ~30 ms +30 mV, Fig. 3A) and voltage dependence (V_{half} –41 mV, Fig. 6B) are consistent with these other $K_V1.4$-containing heteromers.

K_V7 channels contribute a small delayed rectifier in type I and type II hair cells

In $K_V1.8^{-/-}$ HCs, absence of $I_{K,L}$ and I_A revealed smaller delayed rectifier K^+ currents that, unlike $I_{K,L}$, activated positive to resting potential and, unlike I_A, lacked fast inactivation. Candidate channels include members of the K_V7 (KCNQ, M-current) family, which have been identified previously in rodent vestibular HCs (Kharkovets et al., 2000; Rennie et al., 2001; Hurley et al., 2006; Scheffer et al., 2015).

We test for K_V7 contributions in $K_V1.8^{-/-}$ type I HCs, $K_V1.8^{-/-}$ type II HCs, and $K_V1.8^{+/+,+/-}$ type II HCs of multiple ages by applying XE991 at 10 µM (Fig. 7A), a dose selective for K_V7 channels (Brown et al., 2002) and close to the IC_{50} (Alexander et al., 2019). In $K_V1.8^{-/-}$ HCs of both types, 10 µM XE991 blocked about

295 half of the residual K_V conductance (Fig. 7B.1), consistent with K_V7 channels conducting most or all of the
296 non-$K_V1.8$ delayed rectifier current. In all tested HCs (P8-355, median P224), the XE991-sensitive
297 conductance did not inactivate substantially within 200 ms at any voltage, consistent with $K_V7.2$, 7.3, 7.4,
298 and 7.5 currents (Wang, 1998; Kubisch et al., 1999; Schroeder et al., 2000; Jensen et al., 2007; Xu et al.,
299 2007). We refer to this component as $g_{DR}(K_V7)$. The voltage dependence and Gmax density (G_{max}/C_m) of
300 $g_{DR}(K_V7)$ were comparable across HC types and genotypes (Figure 7B.2-4). Although $K_V7.4$ was not
301 detectable in HCs during immunostaining (Fig. 5), $K_V7.4$ has been shown in type I HCs with immunogold
302 labeling (Kharkovets et al., 2000; Hurley et al., 2006).

303 These results are consistent with similar K_V7 channels contributing a relatively small delayed rectifier
304 in both HC types. In addition, the similarity of XE991-sensitive currents of $K_V1.8^{+/+}$ and $K_V1.8^{-/-}$ type II HCs
305 indicates that knocking out $K_V1.8$ did not cause general effects on ion channel expression. We did not test
306 XE991 on $K_V1.8^{+/+,+/-}$ type I HCs because $g_{K,L}$ runs down in ruptured patch recordings (Rüsch and Eatock,
307 1996a; Chen and Eatock, 2000; Hurley et al., 2006), which could contaminate the XE991-sensitive
308 conductance obtained by subtraction.

309 In one striolar $K_V1.8^{-/-}$ type I HC, XE991 also blocked a small conductance that activated negative to
310 rest (Suppl. Fig. 5A-B). This conductance (V_{half} ~= –100 mV, Suppl. Fig. 5C) was detected only in $K_V1.8^{-/-}$
311 type I HCs from the striola (5/23 vs. 0/45 extrastriolar). The V_{half} and $\tau_{deactivation}$ were similar to values
312 reported for $K_V7.4$ channels in cochlear HCs (Wong et al., 2004; Dierich et al., 2020). This very negatively
313 activating K_V7 conductance coexisted with the larger more positively activating K_V7 conductance (Suppl.
314 Fig. 5C) and was too small (<0.5 nS/pF) to contribute significantly to $g_{K,L}$ (~10-100 nS/pF, Fig. 1D).

315

316 ## Other channels

317 While our data are consistent with $K_V1.8$- and K_V7- containing channels carrying most of the outward-
318 rectifying current in mouse utricular hair cells, there is evidence in other preparations for additional
319 channels, including K_V11 (KCNH, Erg) channels in rat utricular type I hair cells (Hurley et al., 2006) and BK
320 (KCNMA1) channels in rat utricle and rat and turtle semicircular canal hair cells (Schweizer et al., 2009;
321 Contini et al., 2020).

322 BK is expressed in mouse utricular hair cells (McInturff et al., 2018; Jan et al., 2021; Orvis et al., 2021).
323 However, Ca^{2+}-dependent currents have not been observed in mouse utricular HCs, and we found little to
324 no effect of the BK-channel blocker iberiotoxin at a dose (100 nM) well beyond the IC_{50}: percent blocked
325 at –30 mV was 2 ± 6% (3 $K_V1.8^{-/-}$ type I HCs); 1 ± 5% (5 $K_V1.8^{+/+,+/-}$ type II HCs); 7% and 14% (2 $K_V1.8^{-/-}$ type
326 II HCs). We also did not see N-shaped I-V curves typical of many Ca^{2+}-dependent K^+ currents. In our
327 ruptured-patch recordings, Ca^{2+}-dependent BK currents and erg channels may have been eliminated by
328 wash-out of the hair cells' small Ca_V currents (Bao et al., 2003) or cytoplasmic second messengers (Hurley
329 et al., 2006).

330 To check whether the constitutive $K_V1.8$ knockout has strong non-specific effects on channel
331 trafficking, we examined the summed HCN and fast inward rectifier currents (I_H and I_{Kir}) at –124 mV, and
332 found them similar across genotypes (Suppl. Fig. 6). The $g_{K,L}$ knockout allowed identification of zonal
333 differences in I_H and I_{Kir} in type I HCs, previously examined in type II HCs (Masetto and Correia, 1997; Levin
334 and Holt, 2012). In type I HCs from both control and null utricles, I_H and I_{Kir} were less prevalent in striola
335 than extrastriola, and, when present, the combined inward current was smaller (Suppl. Fig. 6B).

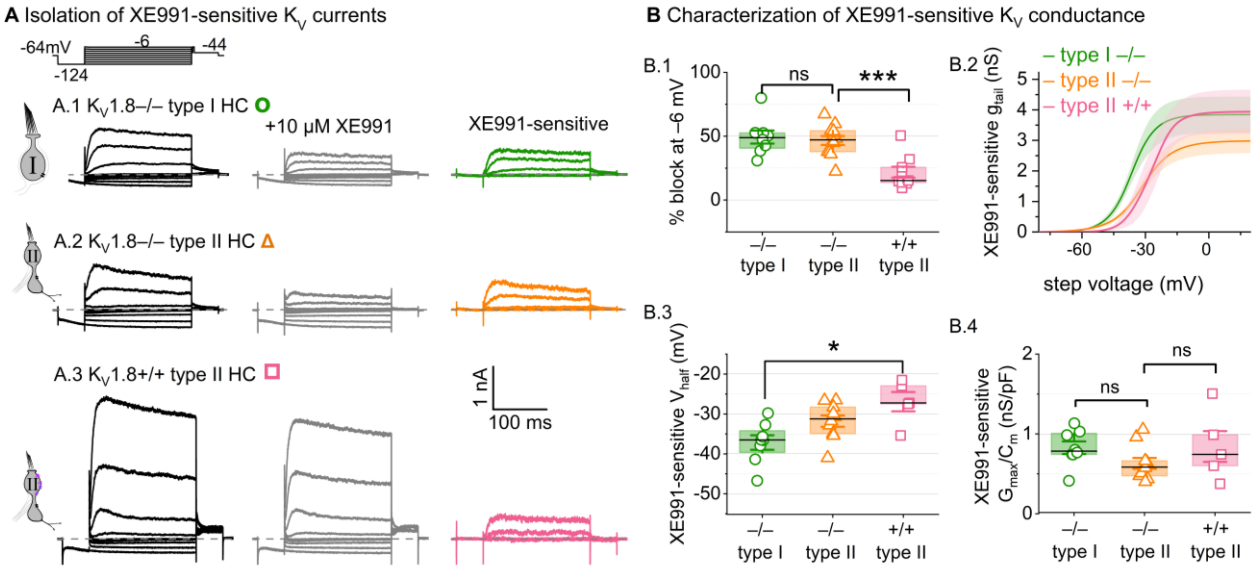

Figure 7. A K_V7-selective blocker, XE991, reduced residual delayed rectifier currents in $K_V1.8^{-/-}$ type I and II HCs.
(A) XE991 (10 µM) partly blocked similar delayed rectifier currents in type I and type II $K_V1.8^{-/-}$ HCs and a type II $K_V1.8^{+/+}$ HC.
(B) Properties of XE991-sensitive conductance, $g_{DR}(K_V7)$. (**B.1**) % Block of steady-state current. (**B.2**) tail G-V curves for $K_V1.8^{-/-}$ type I HCs (n=8), $K_V1.8^{-/-}$ type II HCs (9), and $K_V1.8^{+/+}$ type II HCs (5); mean ± SEM. (**B.3**) V_{half} was less negative in $K_V1.8^{+/+}$ type II than $K_V1.8^{-/-}$ type I HC (p = 0.01, KWA). (**B.4**) Conductance density was similar in all groups (ANOVA, non-significant at 40% power (*left*), 20% power (*right*).

Discussion

We have shown that constitutive knockout of $K_V1.8$ eliminated $g_{K,L}$ in type I HCs, and g_A and much of g_{DR} in type II HCs. $K_V1.8$ immunolocalized specifically to the basolateral membranes of type I and II HCs. We conclude that $K_V1.8$ is a pore-forming subunit of $g_{K,L}$, g_A, and part of g_{DR} [$g_{DR}(K_V1.8)$]. We suggest that fast inactivation of g_A may arise from heteromultimerization of non-inactivating $K_V1.8$ subunits and inactivating $K_V1.4$ subunits. Finally, we showed that a substantial component of the residual delayed rectifier current in both type I and type II HCs comprises K_V7 channels.

$K_V1.8$ is expressed in hair cells from mammalian cochlea (Dierich et al., 2020), avian utricle (Scheibinger et al., 2022), and zebrafish (Erickson and Nicolson, 2015). Our work suggests that in anamniotes, which lack type I cells and $g_{K,L}$, $K_V1.8$ contributes to g_A and g_{DR}, which are widespread in vertebrate HCs (reviewed in Meredith and Rennie, 2016). $K_V1.8$ expression has not been detected in rodent brain but is reported in the pacemaker nucleus of weakly electric fish (Smith et al., 2018).

$K_V1.8$ subunits may form homomultimers to produce $g_{K,L}$ in type I hair cells

Recent single-cell expression studies on mouse utricles (McInturff et al., 2018; Jan et al., 2021; Orvis et al., 2021) have detected just one K_V1 subunit, $K_V1.8$, in mouse type I HCs. Given that $K_V1.8$ can only form multimers with K_V1 family members, and given that $g_{K,L}$ channels are present at very high density (~150

per μm^2 in rat type I, Chen and Eatock, 2000), it stands to reason that most or all of the channels are K_V1.8 homomers. Other evidence is consistent with this proposal. $g_{K,L}$ (Rüsch and Eatock, 1996a) and heterologously expressed K_V1.8 homomers in oocytes (Lang et al., 2000) are non-inactivating and blocked by millimolar Ba^{2+} and 4-aminopyridine and >10 mM TEA. Unlike channels with K_V1.1, K_V1.2, and K_V1.6 subunits, $g_{K,L}$ is not sensitive to 10 nM α-dendrotoxin (Rüsch and Eatock, 1996a). $g_{K,L}$ and heterologously expressed K_V1.8 channels have similar single-channel conductances (~20 pS for $g_{K,L}$ at positive potentials, Chen and Eatock, 2000; 11 pS in oocytes, Lang et al., 2000). $g_{K,L}$ is inhibited—or positively voltage-shifted—by cGMP (Behrend et al., 1997; Chen and Eatock, 2000), presumably via the C-terminal cyclic nucleotide binding domain of K_V1.8.

A major novel property of $g_{K,L}$ is that it activates 30-60 mV negative to type II K_V1.8 conductances and most other low-voltage-activated K_V channels (Ranjan et al., 2019). The very negative activation range is a striking difference between $g_{K,L}$ and known homomeric K_V1.8 channels. Heterologously expressed homomeric K_V1.8 channels have an activation V_{half} of –10 to 0 mV (*X. laevis* oocytes, Lang et al., 2000; CHO cells, Dierich et al., 2020). In cochlear inner HCs, currents attributed to K_V1.8 (by subtraction of other candidates) have a near-zero activation V_{half} (–4 mV, Dierich et al., 2020).

Possible factors in the unusually negative voltage dependence of $g_{K,L}$ include:

1) elevation of extracellular K^+ by the enveloping calyceal terminal, unique to type I HCs (Lim et al., 2011; Contini et al., 2012; Spaiardi et al., 2020; Govindaraju et al., 2023). High K^+ increases conductance though $g_{K,L}$ channels (Contini et al., 2020), perhaps through K^+-mediated relief of C-type inactivation (López-Barneo et al., 1993; Baukrowitz and Yellen, 1995). We note, however, that $g_{K,L}$ is open at rest even in neonatal mouse utricles cultured without innervation (Rüsch et al., 1998) and persists in dissociated type I HCs (Chen and Eatock, 2000; Hurley et al., 2006).

2) The high density of $g_{K,L}$ (~50 nS/pF in striolar $K_V1.8^{+/+}$ HCs) implies close packing of channels, possibly represented by particles (12-14 nm) seen in freeze-fracture electron microscopy of the type I HC membrane (Gulley and Bagger-Sjöbäck, 1979; Sousa et al., 2009). Such close channel packing might hyperpolarize *in situ* voltage dependence of $g_{K,L}$, as proposed for K_V7.4 channels in outer hair cells (Perez-Flores et al., 2020). Type I HC-specific partners that may facilitate this close packing include ADAM11 (McInturff et al., 2018), which clusters presynaptic K_V1.1 and K_V1.2 to enable ephaptic coupling at a cerebellar synapse (Kole et al., 2015).

3) Modulation by accessory subunits. Type I HCs express K_Vβ1 (McInturff et al., 2018; Orvis et al., 2021), an accessory subunit that can confer fast inactivation and hyperpolarize activation V_{half} by ~10 mV. K_Vβ1 might interact with K_V1.8 to shift voltage dependence negatively. Arguments against this possibility include that $g_{K,L}$ lacks fast inactivation (Rüsch and Eatock, 1996a; Hurley et al., 2006; Spaiardi et al., 2017) and that cochlear inner hair cells co-express K_V1.8 and K_Vβ1 (Liu et al., 2018) but their K_V1.8 conductance has a near-0 V_{half} (Dierich et al., 2020).

K_V1.8 subunits may heteromerize with variable numbers of inactivating K_V1.4 subunits to produce g_A and K_V1.8-dependent g_{DR} in type II HCs

The K_V1.8-dependent conductances of type II HCs vary in their fast and slow inactivation. In not showing fast inactivation (Lang et al., 2000; Ranjan et al., 2019; Dierich et al., 2020), heterologously expressed K_V1.8 subunits resemble most other K_V1 family subunits, with the exception of K_V1.4 (for comprehensive review, see Ranjan et al., 2019). K_V1.4 is a good candidate to provide fast inactivation based on immunolocalization and voltage dependence (Figs. 4, 6). We suggest that g_A and g_{DR}(K_V1.8) are K_V1.8-

containing channels that may include a variable number of $K_V1.4$ subunits and $K_V\beta2$ and $K_V\beta1$ accessory subunits.

$K_V1.4$-$K_V1.8$ heteromeric assembly could account for several related observations. The faster $\tau_{Inact,Fast}$ in $K_V1.8^{+/-}$ relative to $K_V1.8^{+/+}$ type II HCs (Fig. 3A.3, Suppl. Fig. 2A.1) could reflect an increased ratio of $K_V1.4$ to $K_V1.8$ subunits and therefore more N-terminal inactivation domains per heteromeric channel. Zonal variation in the extent and speed of N-type inactivation (Fig. 3A) might arise from differential expression of $K_V1.4$. The small fast-inactivating conductance in ~20% of extrastriolar $K_V1.8^{-/-}$ type II HCs (Suppl. Fig. 4) might flow through $K_V1.4$ homomers.

Fast inactivation may also receive contribution from $K_V\beta$ subunits. $K_V\beta1$ is expressed in type II HCs (McInturff et al., 2018; Jan et al., 2021; Orvis et al., 2021), and, together with $K_V1.4$, has been linked to g_A in pigeon vestibular HCs (Correia et al., 2008). $K_V\beta2$, also expressed in type II HCs (McInturff et al., 2018; Orvis et al., 2021), does not confer fast inactivation.

We speculate that g_A and $g_{DR}(K_V1.8)$ have different subunit composition: g_A may include heteromers of $K_V1.8$ with other subunits that confer rapid inactivation, while $g_{DR}(K_V1.8)$ may comprise homomeric $K_V1.8$ channels, given that they do not have N-type inactivation.

$K_V1.8$ relevance for vestibular function

In both type I and type II utricular HCs, $K_V1.8$-dependent channels strongly shape receptor potentials in ways that promote temporal fidelity rather than electrical tuning (Lewis, 1988), consistent with the utricle's role in driving reflexes that compensate for head motions as they occur. This effect is especially pronounced for type I HCs, where the current-step evoked voltage response reproduces the input with great speed and linearity (Fig. 2).

$g_{K,L}$ dominates passive membrane properties in mature $K_V1.8^{+/+,+/-}$ type I HCs such that $K_V1.8^{-/-}$ type I HCs are expected to have receptor potentials with higher amplitudes but lower low-pass corner frequencies, closer to those of type II HCs and immature HCs of all types (Correia et al., 1996; Rüsch and Eatock, 1996a; Songer and Eatock, 2013). In $K_V1.8^{-/-}$ epithelia, we expect the lack of a large basolateral conductance open at rest to reduce the speed and gain of non-quantal transmission, which depends on K^+ ion efflux from the type I HC to change electrical and K^+ potentials in the synaptic cleft (Govindaraju et al., 2023). In hair cells, K^+ enters the mechanosensitive channels of the hair bundle from the K^+-rich apical endolymph and exits through basolateral potassium conductances into the more conventional low-K+ perilymph. For the type I-calyx synapse, having in the hair cell a large, non-inactivating K^+ conductance open across the physiological range of potentials avoids channel gating time and allows for instantaneous changes in current into the cleft and fast afferent signaling (Pastras et al., 2023).

In contrast, mature type II HCs face smaller synaptic contacts and have $K_V1.8$-dependent currents that are not substantially activated at resting potential. They do affect the time course and gain of type II HC responses to input currents, speeding up depolarizing transients, producing a repolarizing rebound during the step, and reducing resonance.

Type I and II vestibular hair cells are closely related, such that adult type II HCs acquire type I-like properties upon deletion of the transcription factor Sox2 (Stone et al., 2021). In normal development of the two cell types, the Kcna10 gene generates biophysically distinct and functionally different ion channels, presenting a natural experiment in functional differentiation of sensory receptor cells.

441
442
443 # Materials and methods

444 ## Preparation

445 All procedures for handling animals followed the NIH Guide for the Care and Use of Laboratory Animals
446 and were approved by the Institutional Animal Care and Use Committees of the University of Chicago and
447 the University of Illinois Chicago. Most mice belonged to a transgenic line with a knockout allele of *Kcna10*
448 (referred to here as $K_V1.8^{-/-}$). Our breeding colony was established with a generous gift of such animals
449 from Sherry M. Jones and Thomas Friedman. These animals are described in their paper (Lee et al., 2013).
450 Briefly, the Texas A&M Institute for Genomic Medicine generated the line on a C57BL/6;129SvEv mixed
451 background by replacing Exon 3 of the *Kcna10* gene with an IRES-bGeo/Purocassette. Mice in our colony
452 were raised on a 12:12h light-dark cycle with access to food and water *ad libitum*.

453 Semi-intact utricles were prepared from ~150 male and ~120 female mice, postnatal days (P) 5-375,
454 for same-day recording. Hair cell K_V channel data were pooled across sexes as most results did not appear
455 to differ by sex; an exception was that $g_{K,L}$ had a more negative V_{half} in males (Suppl. Table 1), an effect not
456 clearly related to age, copy number, or other properties of the activation curve.

457 Preparation, stimulation, and recording methods followed our previously described methods for the
458 mouse utricle (Vollrath and Eatock, 2003). Mice were anesthetized through isoflurane inhalation. After
459 decapitation, each hemisphere was bathed in ice-cold, oxygenated Liebowitz-15 (L15) media. The
460 temporal bone was removed, the labyrinth was cut to isolate the utricle, and the nerve was cut close to
461 the utricle. The utricle was treated with proteinase XXIV (100 μg/mL, ~10 mins, 22°C) to facilitate removal
462 of the otoconia and attached gel layer and mounted beneath two glass rods affixed at one end to a
463 coverslip.
464

465 ## Electrophysiology

466 We used the HEKA Multiclamp EPC10 with Patchmaster acquisition software, filtered by the integrated
467 HEKA filters: a 6-pole Bessel filter at 10 kHz and a second 4-pole Bessel filter at 5 kHz, and sampled at 10-
468 100 kHz. Recording electrodes were pulled (PC-100, Narishige) from soda lime glass (King's Precision Glass
469 R-6) wrapped in paraffin to reduce pipette capacitance. Internal solution contained (in mM) 135 KCl, 0.5
470 $MgCl_2$, 3 MgATP, 5 HEPES, 5 EGTA, 0.1 $CaCl_2$, 0.1 Na-cAMP, 0.1 LiGTP, 5 $Na_2CreatinePO_4$ adjusted to pH
471 7.25 and ~280 mmol/kg by adding ~30 mM KOH. External solution was Liebowitz-15 media supplemented
472 with 10 mM HEPES (pH 7.40, 310 ± 10 mmol/kg). Recording temperature was 22-25°C. Pipette capacitance
473 and membrane capacitance transients were subtracted during recordings with Patchmaster software.
474 Series resistance (8-12 MΩ) was measured after rupture and compensated 60-80% with the amplifier, to
475 final values of ~2 MΩ. Potentials are corrected for remaining (uncompensated) series resistance and liquid
476 junction potential of ~+4 mV, calculated with LJPCalc software (Marino et al., 2014).

477 $K_V1.8^{-/-}$ hair cells appeared healthy in that cells had resting potentials negative to –50 mV, cells lasted
478 a long time (20-30 minutes) in ruptured patch recordings, membranes were not fragile, and extensive
479 blebbing was not seen. Type I HCs with $g_{K,L}$ were transiently hyperpolarized to –90 mV to close $g_{K,L}$ enough
480 to increase R_{input} above 100 MΩ, as needed to estimate series resistance and cell capacitance. The average
481 resting potential, V_{rest}, was –87 mV ± 1 (41), similar to the calculated E_K of –86.1 mV, which is not surprising

given the large K^+ conductance of these cells. V_{rest} is likely more positive *in vivo*, where lower endolymphatic Ca^{2+} increases standing inward current through MET channels.

Voltage protocols to characterize K_V currents differed slightly for type I and II HCs. In standard protocols, the cell is held at a voltage near resting potential (–74 mV in type I and –64 mV in type II), then jumped to –124 mV for 200 ms in type I HCs in order to fully deactivate $g_{K,L}$ and 50 ms in type II HCs in order to remove baseline inactivation of g_A. The subsequent iterated step depolarizations lasted 500 ms in type I HCs because $g_{K,L}$ activates slowly (Wong et al., 2004) and 200 ms in type II HCs, where K_V conductances activate faster. The 50-ms tail voltage was near the reversal potential of HCN channels (–44 mV in mouse utricular hair cells, Rüsch et al., 1998) to avoid HCN current contamination.

G-V (activation) parameters for control type I cells may be expected to vary across experiments on semi-intact (as here), organotypically cultured and denervated (Rüsch et al.,1998), or dissociated-cell preparations, reflecting variation in retention of the calyx (Discussion) and voltage step durations (Wong et al., 2004) which elevate K^+ concentration around the hair cell. Nevertheless, the values we obtained for type I and type II HCs resemble values recorded elsewhere, including experiments in which extra care was taken to avoid extracellular K^+ accumulation (Spaiardi et al., 2017, 2020). The effects of K^+ accumulation on $g_{K,L}$'s steady-state activation curves are small because the operating range is centered on E_K and can be characterized with relatively small currents (Fig. 1A).

Pharmacology

Drug-containing solutions were locally with BASI Bee Hive syringes at a final flow rate of 20 µL/min and a dead time of ~30 s. Global bath perfusion was paused during drug perfusion and recording, and only one cell was used per utricle. Aliquots of test agents in solution were prepared, stored at –20°C, and thawed and added to external solution on the recording day (see Key Resources Table).

Analysis

Data analysis was performed with software from OriginLab (Northampton, MA) and custom MATLAB scripts using MATLAB fitting algorithms.

Fitting voltage dependence and time course of conductances

G-V curves. Current was converted to conductance (G) by dividing by driving force ($V - E_K$; E_K calculated from solutions). For type I HCs, tail G-V curves were generated from current 1 ms after the end of the iterated voltage test step. For type II HCs, peak G-V curves were generated from peak current during the step and steady-state G-V curves were generated from current 1 ms before the end of a 200 ms step. Sigmoidal voltage dependence of G-V curves was fit with the first-order Boltzmann equation (Eq. 1).

$$G(V) = G_{min} + \frac{G_{max}}{1 + e^{\frac{V_{half} - V}{S}}} \qquad (1)$$

V_{half} is the midpoint and S is the slope factor, inversely related to curve steepness near activation threshold.

Activation time course of type II HCs. For type II HCs lacking fast inactivation, outward current activation was fit with Eq. 2.

$$I(t) = I_{SS} * \left(1 - e^{-\frac{t}{\tau w}}\right)^n + I_0 \quad (2)$$

I_{SS} is steady-state current, τ_w is activation time constant, n is the state factor related to the number of closed states (typically constrained to 3), and I_o is baseline current.

To measure activation and inactivation time course of g_A, we used Eq. 3 to fit outward K^+ currents evoked by steps from –125 mV to above –50 mV (Rothman and Manis, 2003b).

$$I(t) = I_{max} * \left(1 - e^{-\frac{t}{\tau w}}\right)^n * (1 - Z * (f * \left(1 - e^{-\frac{t}{\tau_{zf}}}\right) + (1 - f) * \left(1 - e^{-\frac{t}{\tau_{zs}}}\right)) + I_0 \quad (3)$$

Z is total steady-state inactivation ($0 \leq Z < 1$ means incomplete inactivation, which allows the equation to fit non-inactivating delayed rectifier currents), f is the fraction of fast inactivation relative to total inactivation, I_{max} is maximal current, τ_{zf} and τ_{zs} are the fast and slow inactivation time constants. We chose to compare fit parameters at 30 ± 2 mV (91), where fast and slow inactivation were consistently separable and g_A was maximized. In most $K_V1.8^{-/-}$ and some striolar $K_V1.8^{+/+,+/-}$ cells, where fast inactivation was absent and adjusted R^2 did not improve on a single-exponential fit by >0.01, we constrained f in Eq. 3 to 0 to avoid overfitting.

For *Peak* G-V relations, peak conductance was taken from fitted curves (Eqs. 2 and 3). To construct '*Steady-state'* G-V relations, we used current at 200 ms (6 ± 1 % (94) greater than steady-state estimated from fits to Eq. 3 (Fig. 3C-D)).

Percent inactivation was calculated at 30 mV with Eq. 4 :

$$\%\ Inactivation = (I_{Peak} - I_{SS})/I_{Peak} \quad (4)$$

I_{Peak} is maximal current, and I_{SS} is current at the end of a 200 ms voltage step.

The electrical resonance of type II HCs was quantified by fitting voltage responses to current injection steps (Songer and Eatock, 2013). We fit Eq. 5, a damped sinusoid, to the voltage trace from half-maximum of the initial depolarizing peak until the end of the current step.

$$V(t) = V_{ss} + V_p * e^{-\frac{t}{\tau e}} * \sin(2\pi f_e - \theta) \quad (5)$$

V_{SS} is steady-state voltage, V_p is the voltage of the peak response, τ_e is the decay time constant, f_e is the fundamental frequency, and θ is the phase angle shift.

Quality factor, Q_e, was calculated with Eq. 6 (Crawford and Fettiplace, 1981).

$$Q_e = [(\pi f_e \tau_e)^2 + 0.25]^{1/2} \quad (6)$$

Statistics

We give means ± SEM for normally-distributed data, and otherwise, median and range. Data normality was assessed with the Shapiro-Wilk test for n<50 and the Kolmogorov-Smirnov test for n>50. To assess homogeneity of variance we used Levene's test. With homogeneous variance, we used two-way ANOVA for genotype and zone with the posthoc Tukey's test. When variance was non-homogeneous, we used one-way Welch ANOVA with the posthoc Games-Howell test. For data that were not normally distributed, we used the non-parametric one-way Kruskal-Wallis ANOVA (KWA) with posthoc Dunn's test. Effect size

557 is Hedge's g (g). For age dependence, we used partial correlation coefficients controlling for genotype and
558 zone. Statistical groups may have different median ages, but all have overlapping age ranges. In figures,
559 asterisks represent p-value ranges as follows: *, $p<0.05$; **, $p<0.01$; ***, $p<0.001$; ****, $p<0.0001$.
560

561 ## Immunohistochemistry

562 Mice were anesthetized with Nembutal (80 mg/kg), then perfused transcardially with 40mL of
563 physiological saline containing heparin (400 IU), followed by 2 mL/g body weight fixative (4%
564 paraformaldehyde, 1% picric acid, and 5% sucrose in 0.1 M phosphate buffer at pH 7.4, sometimes with
565 1% acrolein). Vestibular epithelia were dissected in phosphate buffer, and tissues were cryoprotected in
566 30% sucrose-phosphate buffer overnight at 4°C. Otoconia were dissolved with Cal-Ex (Fisher Scientific) for
567 10 min. Frozen sections (35 µm) were cut with a sliding microtome. Immunohistochemistry was
568 performed on free-floating sections. Tissues were first permeabilized with 4% Triton X-100 in PBS for 1 h
569 at room temperature, then incubated with 0.5% Triton X-100 in a blocking solution of 0.5% fish gelatin
570 and 1% BSA for 1 h at room temperature. Sections were incubated with 2-3 primary antibodies for 72 h
571 at 4°C and with 2-3 secondary antibodies. Sections were rinsed with PBS between and after incubations
572 and mounted on slides in Mowiol (Calbiochem).
573

Table 6. Key Resources Table

Antibody	Source	Catalog Number	Lot Number	Dilution
Rabbit anti-K_V1.8	Alomone	APC-157	0102	1:200 or 1:400
Mouse anti-K_V1.4	NeuroMab	P15385	5HK-05	1:400
Mouse IGg2a-conjugated anti-Tuj1	Covance	MMS-435P	B205808	1:300
Goat anti-calretinin	Millipore	AB1550	9669	1:600
Mouse IgG1-conjugated anti-K_V7.4	NeuroMab	2HK-65		1:200
Donkey anti-Rabbit Secondary Antibody, Alexa Fluor 594	Invitrogen	A21207	8652	1:200
Donkey anti-Goat 488 nm	Invitrogen	A21125	1920483	1:200
Goat anti-Mouse IgG1 594	Invitrogen	A11055	1869589	1:200
Chemicals and Peptides	**Source**	**Catalog Number**	**Diluent**	
Iberiotoxin	Alomone	STI-400	Water	
XE991 dihydrochloride	Sigma	X2254	Water	
ZD7288	Tocris	APN18035-2	Water	
Bovine serum albumin	Fisher	BP671	water	

574
575
576
577

578 # Data Availability

579 Data used in this study are available on Dryad (https://doi.org/10.5061/dryad.37pvmcvrw).

Acknowledgements

This study was supported by NIH grant R01 DC012347 to RAE and AL and an NSF Graduate Research Fellowship to HRM. We thank Drs. Thomas Friedman and Sherri Jones for the generous gift of the $K_V1.8^{-/-}$ mouse line, and Drs. Zheng-Yi Chen and Deborah I. Scheffer for bringing the expression of this subunit in mouse vestibular hair cells to our attention.

We acknowledge Dr. Vicente Lumbreras for insights from his prior experiments on g_A in mouse utricular hair cells, and thank him for helpful further discussions.

We acknowledge Steven D. Price for his help with immunocytochemistry.

We thank Drs. Rebecca Lim and Ebenezer Yamoah for their critical feedback on the manuscript, and Drs. Rob Raphael and Aravind Chenrayan Govindaraju for feedback and many helpful discussions. We thank Drs. Joe Burns, Gabi Pregernig, and Lars Becker (Decibel Therapeutics, Inc.) for helpful discussions.

Author Contributions

HRM designed and performed experiments, analyzed data, and wrote the paper; RAE helped design experiments, analyze data, and write the paper; AL performed immunohistochemistry experiments and reviewed and edited the manuscript.

References

Alexander SPH et al. (2019) The Concise Guide to Pharmacology 2019/20: Ion channels. Br J Pharmacol 176 Available at: https://onlinelibrary.wiley.com/doi/10.1111/bph.14749 [Accessed April 12, 2022].

Al-Sabi A, Kaza S, Le Berre M, O'Hara L, Bodeker M, Wang J, Dolly JO (2011) Position-dependent attenuation by Kv1.6 of N-type inactivation of Kv1.4-containing channels. Biochem J 438:389–396.

Ashmore JF (1983) Frequency tuning in a frog vestibular organ. Nature 304:536–538.

Bao H, Wong WH, Goldberg JM, Eatock RA (2003) Voltage-Gated Calcium Channel Currents in Type I and Type II Hair Cells Isolated From the Rat Crista. J Neurophysiol 90:155–164.

Baukrowitz T, Yellen G (1995) Modulation of K+ current by frequency and external [K+]: A tale of two inactivation mechanisms. Neuron 15:951–960.

Behrend O, Schwark C, Kunihiro T, Strupp M (1997) Cyclic GMP inhibits and shifts the activation curve of the delayed rectifier (I(K1)) of type I mammalian vestibular hair cells. NeuroReport 8:2687–2690.

Brown DA, Selyanko AA, Hadley JK, Tatulian L (2002) Some Pharmacological Properties Of Neural KCNQ Channels. Neurophysiology 34:91–94.

Carlisle FA, Steel KP, Lewis MA (2012) Specific expression of Kcna10, Pxn and Odf2 in the organ of Corti. Gene Expression Patterns 12:172–179.

616 Chen JWY, Eatock RA (2000) Major Potassium Conductance in Type I Hair Cells from Rat Semicircular
617 Canals: Characterization and Modulation by Nitric Oxide. J Neurophysiol 84:139–151.

618 Contini D, Holstein GR, Art JJ (2020) Synaptic cleft microenvironment influences potassium permeation
619 and synaptic transmission in hair cells surrounded by calyx afferents in the turtle. J Physiol
620 598:853–889.

621 Contini D, Price SD, Art JJ (2017) Accumulation of K^+ in the synaptic cleft modulates activity by
622 influencing both vestibular hair cell and calyx afferent in the turtle: K^+ modulation of synaptic
623 transmission between hair cell and afferent. J Physiol 595:777–803.

624 Contini D, Zampini V, Tavazzani E, Magistretti J, Russo G, Prigioni I, Masetto S (2012) Intercellular K^+
625 accumulation depolarizes Type I vestibular hair cells and their associated afferent nerve calyx.
626 Neuroscience 227:232–246.

627 Correia MJ, Lang DG (1990) An electrophysiological comparison of solitary type I and type II vestibular
628 hair cells. Neuroscience Letters 116:106–111.

629 Correia MJ, Ricci AJ, Rennie KJ (1996) Filtering Properties of Vestibular Hair Cells: An Update. Ann NY
630 Acad Sci 781:138–149.

631 Correia MJ, Weng T, Prusak D, Wood TG (2008) Kvβ1.1 Associates with Kv1.4 in Chinese Hamster Ovary
632 Cells and Pigeon Type II Vestibular Hair Cells and Enhances the Amplitude, Inactivation and
633 Negatively Shifts the Steady-State Inactivation Range. Neuroscience 152:809–820.

634 Crawford AC, Fettiplace R (1981) An electrical tuning mechanism in turtle cochlear hair cells. J Physiol
635 312:377–412.

636 Desai SS, Zeh C, Lysakowski A (2005) Comparative Morphology of Rodent Vestibular Periphery. I.
637 Saccular and Utricular Maculae. J Neurophysiol 93:251–266.

638 Dierich M, Altoè A, Koppelmann J, Evers S, Renigunta V, Schäfer MK, Naumann R, Verhulst S, Oliver D,
639 Leitner MG (2020) Optimized Tuning of Auditory Inner Hair Cells to Encode Complex Sound
640 through Synergistic Activity of Six Independent K+ Current Entities. Cell Reports 32:107869.

641 Dwenger MM, Raph SM, Baba SP, Moore JB, Nystoriak MA (2022) Diversification of Potassium Currents
642 in Excitable Cells via Kvβ Proteins. Cells 11:2230.

643 Eatock RA, Songer JE (2011) Vestibular Hair Cells and Afferents: Two Channels for Head Motion Signals.
644 Annu Rev Neurosci 34:501–534.

645 Erickson T, Nicolson T (2015) Identification of sensory hair-cell transcripts by thiouracil-tagging in
646 zebrafish. BMC Genomics 16:842.

647 Fettiplace R (1987) Electrical tuning of hair cells in the inner ear. TINS 10:5.

648 Géléoc GS, Risner J, Holt JR (2004) Developmental Acquisition of Voltage-Dependent Conductances and
649 Sensory Signaling in Hair Cells of the Embryonic Mouse Inner Ear. J Neurosci 24:11148–11159.

650 Goldberg JM (2000) Afferent diversity and the organization of central vestibular pathways. Exp Brain Res
651 130:277–297.

652 González-Garrido A, Pujol R, López-Ramírez O, Finkbeiner C, Eatock RA, Stone JS (2021) The
653 Differentiation Status of Hair Cells That Regenerate Naturally in the Vestibular Inner Ear of the
654 Adult Mouse. J Neurosci 41:7779–7796.

655 Govindaraju AC, Quraishi IH, Lysakowski A, Eatock RA, Raphael RM (2023) Nonquantal transmission at
656 the vestibular hair cell–calyx synapse: K_{LV} currents modulate fast electrical and slow K^+
657 potentials. Proc Natl Acad Sci USA 120:e2207466120.

658 Gulley A, Bagger-Sjöbäck D (1979) Freeze-fracture studies on the synapse between the type I hair cells
659 and the calyceal terminal in the guinea-pig vestibular system. J Neurocytol 8:591–603.

660 Holt JR, Stauffer EA, Abraham D, Geleoc GSG (2007) Dominant-Negative Inhibition of M-Like Potassium
661 Conductances in Hair Cells of the Mouse Inner Ear. J Neurosci 27:8940–8951.

662 Horwitz GC, Risner-Janiczek JR, Jones SM, Holt JR (2011) HCN Channels Expressed in the Inner Ear Are
663 Necessary for Normal Balance Function. J Neurosci 31:16814–16825.

664 Hudspeth AJ, Lewis RS (1988) A model for electrical resonance and frequency tuning in saccular hair cells
665 of the bull-frog, Rana catesbeiana. J Physiol 400:275–297.

666 Hurley KM, Gaboyard S, Zhong M, Price SD, Wooltorton JRA, Lysakowski A, Eatock RA (2006) M-Like K^+
667 Currents in Type I Hair Cells and Calyx Afferent Endings of the Developing Rat Utricle. Journal of
668 Neuroscience 26:10253–10269.

669 Imbrici P, D'Adamo MC, Kullmann DM, Pessia M (2006) Episodic ataxia type 1 mutations in the *KCNA1*
670 gene impair the fast inactivation properties of the human potassium channels Kv1.4-1.1/Kvβ1.1
671 and Kv1.4-1.1/Kvβ1.2. Eur J Neurosci 24:3073–3083.

672 Jan TA, Eltawil Y, Ling AH, Chen L, Ellwanger DC, Heller S, Cheng AG (2021) Spatiotemporal dynamics of
673 inner ear sensory and non-sensory cells revealed by single-cell transcriptomics. Cell Reports
674 36:109358.

675 Jensen HS, Grunnet M, Olesen S-P (2007) Inactivation as a New Regulatory Mechanism for Neuronal Kv7
676 Channels. Biophys J 92:2747–2756.

677 Kharkovets T, Hardelin J-P, Safieddine S, Schweizer M, El-Amraoui A, Petit C, Jentsch TJ (2000) KCNQ4, a
678 K^+ channel mutated in a form of dominant deafness, is expressed in the inner ear and the central
679 auditory pathway. Proc Natl Acad Sci USA 97:4333–4338.

680 Kole MJ, Qian J, Waase MP, Klassen TL, Chen TT, Augustine GJ, Noebels JL (2015) Selective Loss of
681 Presynaptic Potassium Channel Clusters at the Cerebellar Basket Cell Terminal Pinceau in
682 Adam11 Mutants Reveals Their Role in Ephaptic Control of Purkinje Cell Firing. J Neurosci
683 35:11433–11444.

684 Kubisch C, Schroeder BC, Friedrich T, Lütjohann B, El-Amraoui A, Marlin S, Petit C, Jentsch TJ (1999)
685 KCNQ4, a Novel Potassium Channel Expressed in Sensory Outer Hair Cells, Is Mutated in
686 Dominant Deafness. Cell 96:437–446.

687 Lang R, Lee G, Liu W, Tian S, Rafi H, Orias M, Segal AS, Desir GV (2000) KCNA10: A novel ion channel
688 functionally related to both voltage-gated potassium and CNG cation channels. American
689 Journal of Physiology - Renal Physiology 278.

690 Lee SI, Conrad T, Jones SM, Lagziel A, Starost MF, Belyantseva IA, Friedman TB, Morell RJ (2013) A null
691 mutation of mouse Kcna10 causes significant vestibular and mild hearing dysfunction. Hear Res
692 300:1–9.

693 Levin ME, Holt JR (2012) The function and molecular identity of inward rectifier channels in vestibular
694 hair cells of the mouse inner ear. J Neurophysiol 108:175–186.

695 Lewis ER (1988) Tuning in the bullfrog ear. Biophysical Journal 53:441–447.

696 Lim R, Kindig AE, Donne SW, Callister RJ, Brichta AM (2011) Potassium accumulation between type I hair
697 cells and calyx terminals in mouse crista. Exp Brain Res 210:607–621.

698 Liu H, Chen L, Giffen KP, Stringham ST, Li Y, Judge PD, Beisel KW, He DZZ (2018) Cell-Specific
699 Transcriptome Analysis Shows That Adult Pillar and Deiters' Cells Express Genes Encoding
700 Machinery for Specializations of Cochlear Hair Cells. Front Mol Neurosci 11:356.

701 López-Barneo J, Hoshi T, Heinemann SH, Aldrich RW (1993) Effects of external cations and mutations in
702 the pore region on C-type inactivation of Shaker potassium channels. Recept Channels 1:61–71.

703 Lysakowski A, Gaboyard-Niay S, Calin-Jageman I, Chatlani S, Price SD, Eatock RA (2011) Molecular
704 Microdomains in a Sensory Terminal, the Vestibular Calyx Ending. J Neurosci 31:10101–10114.

705 Lysakowski A, Goldberg JM (2004) Morphophysiology of the vestibular periphery. In: The Vestibular
706 System, pp 57–152 Springer Hearing and Auditory Research. Springer New York. Available at:
707 https://doi.org/10.1007/0-387-21567-0_3.

708 Marino M, Misuri L, Brogioli D (2014) A new open source software for the calculation of the liquid
709 junction potential between two solutions according to the stationary Nernst-Planck equation.
710 Available at: http://arxiv.org/abs/1403.3640 [Accessed October 23, 2023].

711 Masetto S, Correia MJ (1997) Electrophysiological Properties of Vestibular Sensory and Supporting Cells
712 in the Labyrinth Slice Before and During Regeneration. J Neurophysiol 78:1913–1927.

713 McInturff S, Burns JC, Kelley MW (2018) Characterization of spatial and temporal development of Type I
714 and Type II hair cells in the mouse utricle using new cell-type-specific markers. Biol Open
715 7:bio038083.

716 Meredith FL, Rennie KJ (2016) Channeling your inner ear potassium: K+ channels in vestibular hair cells.
717 Hear Res 338:40–51.

718 Mitra K, Ubarretxena-Belandia I, Taguchi T, Warren G, Engelman DM (2004) Modulation of the bilayer
719 thickness of exocytic pathway membranes by membrane proteins rather than cholesterol. Proc
720 Natl Acad Sci USA 101:4083–4088.

721 Orvis J et al. (2021) gEAR: Gene Expression Analysis Resource portal for community-driven, multi-omic
722 data exploration. Nat Methods 18:843–844.

723 Pastras CJ, Curthoys IS, Asadnia M, McAlpine D, Rabbitt RD, Brown DJ (2023) Evidence that ultrafast non-
724 quantal transmission underlies synchronized vestibular action potential generation. J
725 Neurosci:JN-RM-1417-23.

726 Perez-Flores MC, Lee JH, Park S, Zhang X-D, Sihn C-R, Ledford HA, Wang W, Kim HJ, Timofeyev V, Yarov-
727 Yarovoy V, Chiamvimonvat N, Rabbitt RD, Yamoah EN (2020) Cooperativity of K_v 7.4 channels
728 confers ultrafast electromechanical sensitivity and emergent properties in cochlear outer hair
729 cells. Sci Adv 6:eaba1104.

730 Pujol R, Pickett SB, Nguyen TB, Stone JS (2014) Large basolateral processes on type II hair cells are novel
731 processing units in mammalian vestibular organs: Basolateral Processes of Type II Hair Cells. J
732 Comp Neurol 522:3141–3159.

733 Ramanathan K, Fuchs PA (2002) Modeling Hair Cell Tuning by Expression Gradients of Potassium
734 Channel. Biophys J 82:64–72.

735 Ranjan R, Logette E, Marani M, Herzog M, Tache V, Scantamburlo E, Buchilier V, Markram H (2019) A
736 Kinetic Map of the Homomeric Voltage-Gated Potassium Channel (Kv) Family. Front Cell
737 Neurosci 13:358.

738 Rennie KJ, Correia MJ (1994) Potassium currents in mammalian and avian isolated type I semicircular
739 canal hair cells. J Neurophysiol 71:317–329.

740 Rennie KJ, Weng T, Correia MJ (2001) Effects of KCNQ channel blockers on K^+ currents in vestibular hair
741 cells. Am J Physiol Cell Physiol 280:C473–C480.

742 Ricci AJ, Rennie KJ, Correia MJ (1996) The delayed rectifier, IKI, is the major conductance in type I
743 vestibular hair cells across vestibular end organs. Pflüg Arch Eur J Physiol 432:34–42.

744 Rothman JS, Manis PB (2003) Kinetic Analyses of Three Distinct Potassium Conductances in Ventral
745 Cochlear Nucleus Neurons. J Neurophysiol 89:3083–3096.

746 Rüsch A, Eatock RA (1996a) A delayed rectifier conductance in type I hair cells of the mouse utricle. J
747 Neurophysiol 76:995–1004.

748 Rüsch A, Eatock RA (1996b) Voltage Responses of Mouse Utricular Hair Cells to Injected Currents. Ann
749 NY Acad Sci 781:71–84.

750 Rüsch A, Lysakowski A, Eatock RA (1998) Postnatal development of type I and type II hair cells in the
751 mouse utricle: Acquisition of voltage-gated conductances and differentiated morphology.
752 Journal of Neuroscience 18:7487–7501.

753 Scheffer DI, Shen J, Corey DP, Chen Z-Y (2015) Gene Expression by Mouse Inner Ear Hair Cells during
754 Development. J Neurosci 35:6366–6380.

755 Scheibinger M, Janesick A, Benkafadar N, Ellwanger DC, Jan TA, Heller S (2022) Cell-type identity of the
756 avian utricle. Cell Reports 40:111432.

757 Schroeder BC, Hechenberger M, Weinreich F, Kubisch C, Jentsch TJ (2000) KCNQ5, a Novel Potassium
758 Channel Broadly Expressed in Brain, Mediates M-type Currents. Journal of Biological Chemistry
759 275:24089–24095.

760 Schweizer FE, Savin D, Luu C, Sultemeier DR, Hoffman LF (2009) Distribution of high-conductance
761 calcium-activated potassium channels in rat vestibular epithelia. J Comp Neurol 517:134–145.

762 Smith GT, Proffitt MR, Smith AR, Rusch DB (2018) Genes linked to species diversity in a sexually
763 dimorphic communication signal in electric fish. J Comp Physiol A 204:93–112.

764 Songer JE, Eatock RA (2013) Tuning and Timing in Mammalian Type I Hair Cells and Calyceal Synapses. J
765 Neurosci 33:3706–3724.

766 Sousa AD, Andrade LR, Salles FT, Pillai AM, Buttermore ED, Bhat MA, Kachar B (2009) The Septate
767 Junction Protein Caspr Is Required for Structural Support and Retention of KCNQ4 at Calyceal
768 Synapses of Vestibular Hair Cells. J Neurosci 29:3103–3108.

769 Spaiardi P, Tavazzani E, Manca M, Milesi V, Russo G, Prigioni I, Marcotti W, Magistretti J, Masetto S
770 (2017) An allosteric gating model recapitulates the biophysical properties of $I_{K,L}$ expressed in
771 mouse vestibular type I hair cells: Allosteric gating of $I_{K,L}$. J Physiol 595:6735–6750.

772 Spaiardi P, Tavazzani E, Manca M, Russo G, Prigioni I, Biella G, Giunta R, Johnson SL, Marcotti W,
773 Masetto S (2020) K+ Accumulation and Clearance in the Calyx Synaptic Cleft of Type I Mouse
774 Vestibular Hair Cells. Neuroscience 426:69–86.

775 Spitzmaul G, Tolosa L, Winkelman BHJ, Heidenreich M, Frens MA, Chabbert C, de Zeeuw CI, Jentsch TJ
776 (2013) Vestibular Role of KCNQ4 and KCNQ5 K+ Channels Revealed by Mouse Models*. Journal
777 of Biological Chemistry 288:9334–9344.

778 Stone JS, Pujol R, Nguyen TB, Cox BC (2021) The Transcription Factor Sox2 Is Required to Maintain the
779 Cell Type-Specific Properties and Innervation of Type II Vestibular Hair Cells in Adult Mice. J
780 Neurosci 41:6217–6233.

781 Stühmer W, Ruppersberg JP, Schröter KH, Sakmann B, Stocker M, Giese KP, Perschke A, Baumann A,
782 Pongs O (1989) Molecular basis of functional diversity of voltage-gated potassium channels in
783 mammalian brain. EMBO J 8:3235–3244.

784 Vollrath MA, Eatock RA (2003) Time course and extent of mechanotransducer adaptation in mouse
785 utricular hair cells: Comparison with frog saccular hair cells. Journal of Neurophysiology
786 90:2676–2689.

787 Wang H (1998) KCNQ2 and KCNQ3 Potassium Channel Subunits: Molecular Correlates of the M-Channel.
788 Science 282:1890–1893.

789 Wersäll J (1956) Studies on the structure and innervation of the sensory epithelium of the cristae
790 ampulares in the guinea pig; a light and electron microscopic investigation. Acta Otolaryngol
791 Suppl 126:1–85.

792 Wong WH, Hurley KM, Eatock RA (2004) Differences Between the Negatively Activating Potassium
793 Conductances of Mammalian Cochlear and Vestibular Hair Cells. J Assoc Res Otolaryngol 5:270–
794 284.

795 Xu T, Nie L, Zhang Y, Mo J, Feng W, Wei D, Petrov E, Calisto LE, Kachar B, Beisel KW, Vazquez AE, Yamoah
796 EN (2007) Roles of Alternative Splicing in the Functional Properties of Inner Ear-specific KCNQ4
797 Channels. J Biol Chem 282:23899–23909.

798 Yao X (2002) Expression of KCNA10, a Voltage-Gated K Channel, in Glomerular Endothelium and at the
799 Apical Membrane of the Renal Proximal Tubule. Journal of the American Society of Nephrology
800 13:2831–2839.

801

802

Supplemental Figures

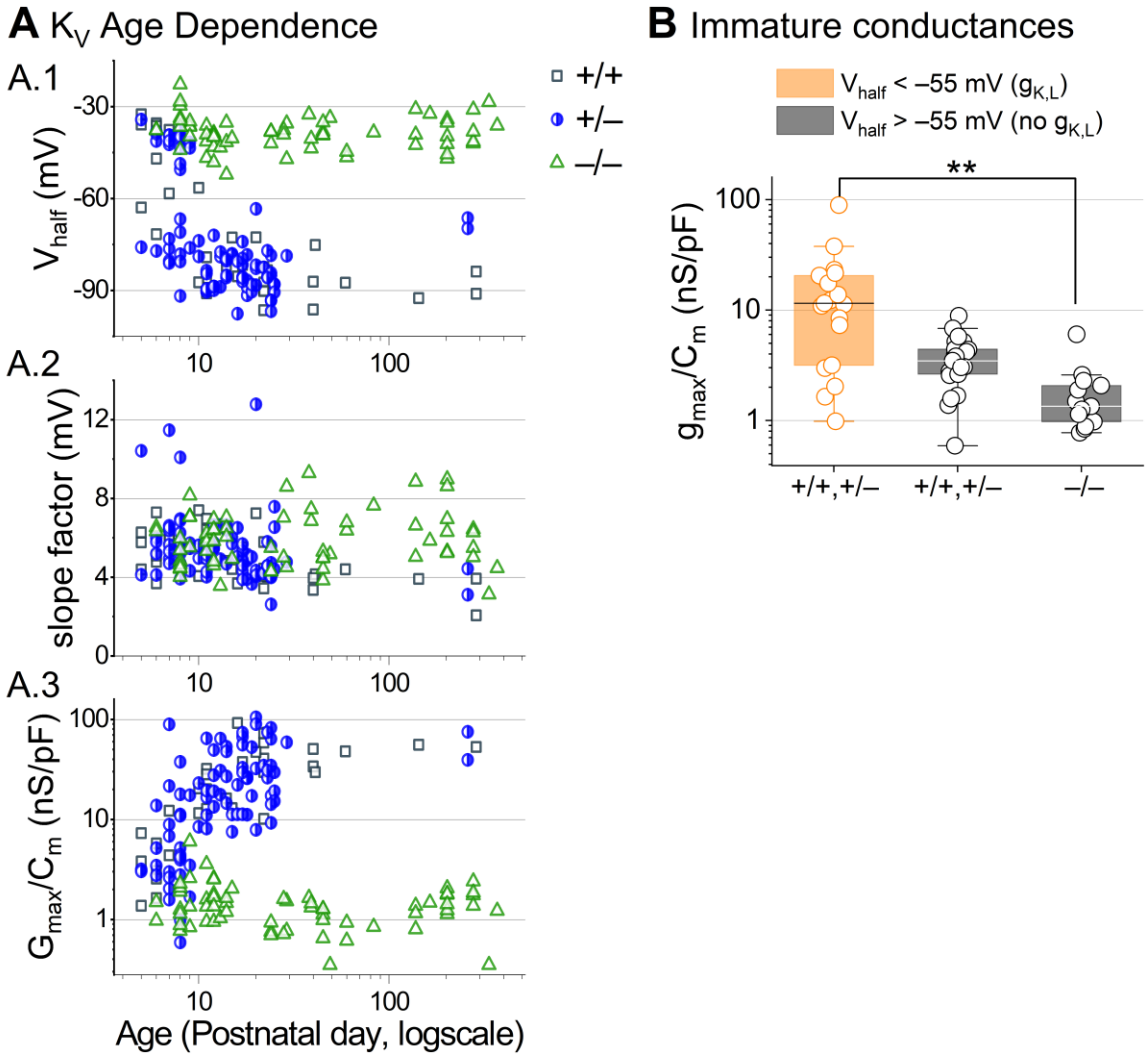

Supplemental Figure 1. Developmental changes in type I HC K_V conductances.
(**A**) Parameters from Boltzmann fits of tail G-V relations for type I HCs plotted against age.
(**B**) Conductance density is similar in young (P5-P10) type I HCs that lack $g_{K,L}$. $g_{K,L}$ is defined here as having a V_{half} negative to –55 mV. $K_V1.8^{+/+,+/-}$ *with* $g_{K,L}$, 17 ± 5 nS/pF (19); $K_V1.8^{+/+,+/-}$ *without* $g_{K,L}$, 3.7 ± 0.4 nS/pF (22); $K_V1.8^{-/-}$, 1.8 ± 0.4 nS/pF (13). $K_V1.8^{+/+,+/-}$ *with* $g_{K,L}$ vs. $K_V1.8^{-/-}$: p = 0.007, KWA, g 1.0.

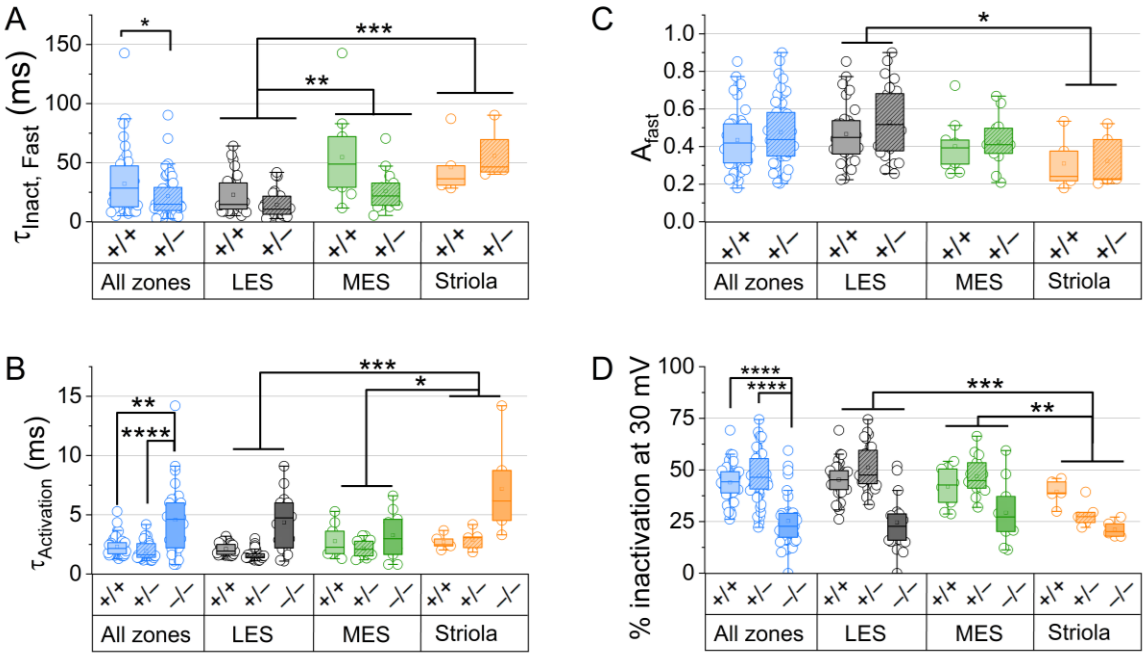

Supplemental Figure 2. **For type II HCs older than P12, K_V conductance activation and inactivation differed across zones and genotypes.**

(**A**) $\tau_{inact,Fast}$ at 30 mV was fastest in LES in $K_V1.8^{+/+}$ and $K_V1.8^{+/-}$ HCs, and faster in $K_V1.8^{+/-}$ than $K_V1.8^{+/+}$ HCs (see Table 3 for p-values).

(**B**) Fast inactivation was a larger fraction of the total in LES than striola.

(**C**) τ_{Act} at 30 mV was slower in $K_V1.8^{-/-}$ than $K_V1.8^{+/+}$ and $K_V1.8^{+/-}$, and slower in striola than LES and MES.

(**D**) Percent inactivation at 30 mV was lowest in striola (zone effect), and lowest in $K_V1.8^{-/-}$ HCs (genotype effect).

807

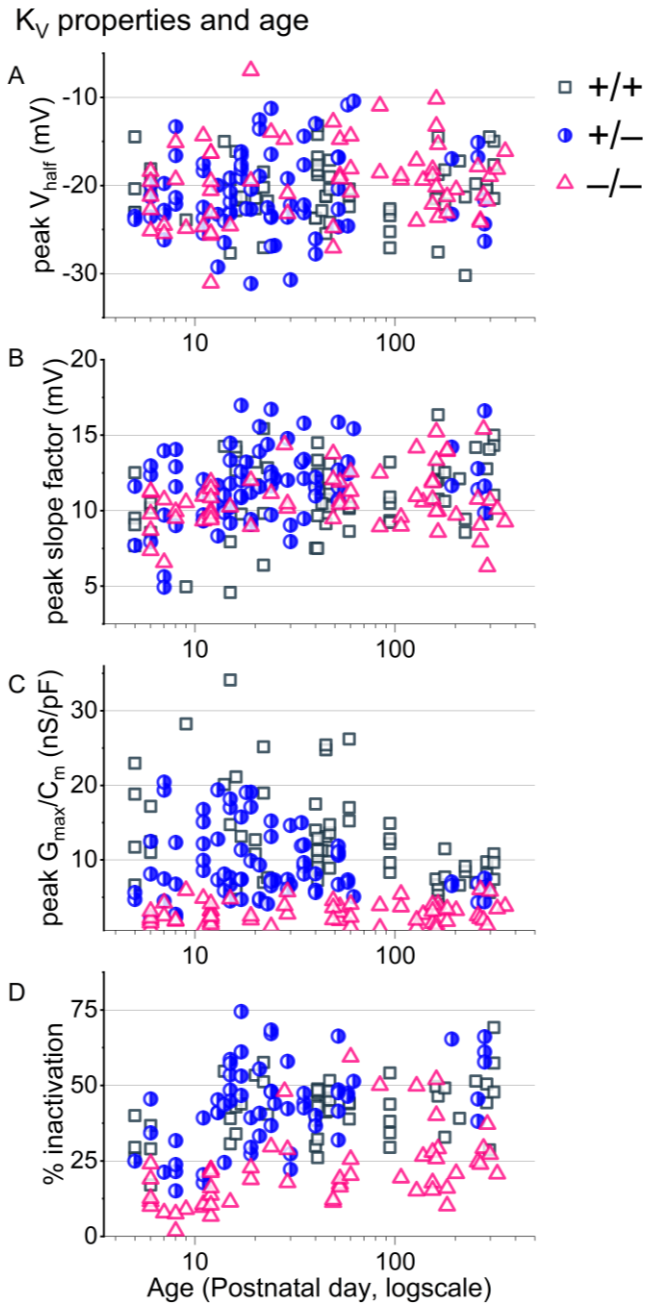

Supplemental Figure 3. For type II HCs older than P12, K_V conductances were stable. (**A-C**) Parameters from Boltzmann fits of peak G-V relations and (**D**) % inactivation at +30 mV plotted against age from all zones. Overlaid curves are smoothing cubic β-splines. Note the seven extrastriolar $K_V1.8^{-/-}$ type II HCs with % inactivation >30%.

808
809
810
811
812

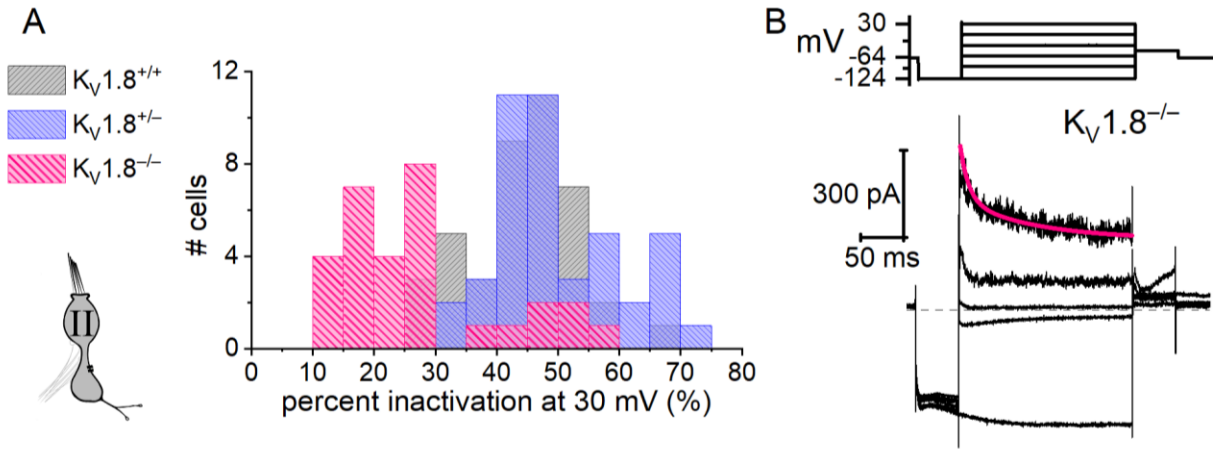

Supplemental Figure 4. A minority of extrastriolar $K_V1.8^{-/-}$ type II HCs had a very small fast-inactivating outward rectifier current.

(**A**) All extrastriolar $K_V1.8^{+/+,+/-}$ type II HCs inactivated by >30%. Most mature (>P12) extrastriolar $K_V1.8^{-/-}$ type II HCs inactivated by <30% but some inactivated by >30% (7/30, 23%) because they had fast inactivation (B).

(**B**) Exemplar residual fast inactivation ($\tau_{FastInact}$ = 10 ms at +30 mV). For the 7 cells in this group, $\tau_{FastInact}$ = 30 ± 6 ms, amplitude of fast inactivation = 310 ± 70 pA; activation peak V_{half} = –15 ± 2 mV and slope factor = 12.4 ± 0.9 mV. These parameters are similar to g_A but for the much smaller conductance (one-way ANOVAs).

813
814
815
816
817
818
819
820
821

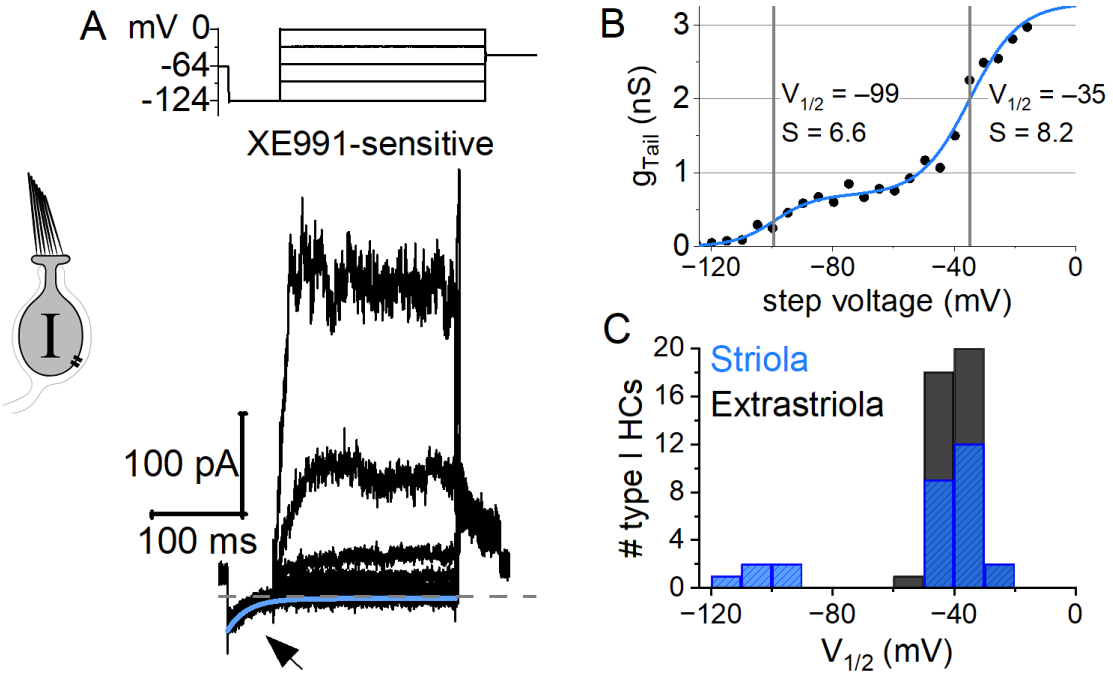

Supplemental Figure 5. A minority of striolar $K_V1.8^{-/-}$ type I HCs had a small low-voltage-activated outward rectifier current in addition to a more positively activating outward rectifier.

(**A**) Low-voltage-activated current from one cell was isolated by subtraction with 10 µM XE991 (P39), indicating that it was carried by K_V7 channels. Deactivation of XE991-sensitive current evoked by step from –64 mV to –124 mV *(arrow)* was fit with exponential decay (τ = 21 ms). (**B**) XE991-sensitive tail G-V curve of the XE991-blocked conductance (A) was fit with a sum of two Boltzmann equations: $G(V) = A_1/(1 + \exp((V_{half,1} - V)/S_1)) + A_2/(1 + \exp((V_{half,2} - V)/S_2))$.

(**C**) The low-voltage-activated $V_{half,1}$ component was only seen in striolar $K_V1.8^{-/-}$ type I HCs, and even there in the minority: 5/23; 22%; P6-P370). It was always seen together with a more positively activating outward rectifier. Boltzmann parameters, including (B): $A_1/(A_1+A_2) = 0.15 \pm 0.04$, $V_{half,1} = -106 \pm 5$ mV (n=5), $S_1 = 3.8 \pm 0.8$ mV, $V_{half,2} = -41 \pm 1$ mV, $S_2 = 7 \pm 1$ mV. Ages: P11, 39, 202, 202, 202. No extrastriolar type I HCs (0/45; P6-277) had a double activation tail G-V curve.

822
823
824

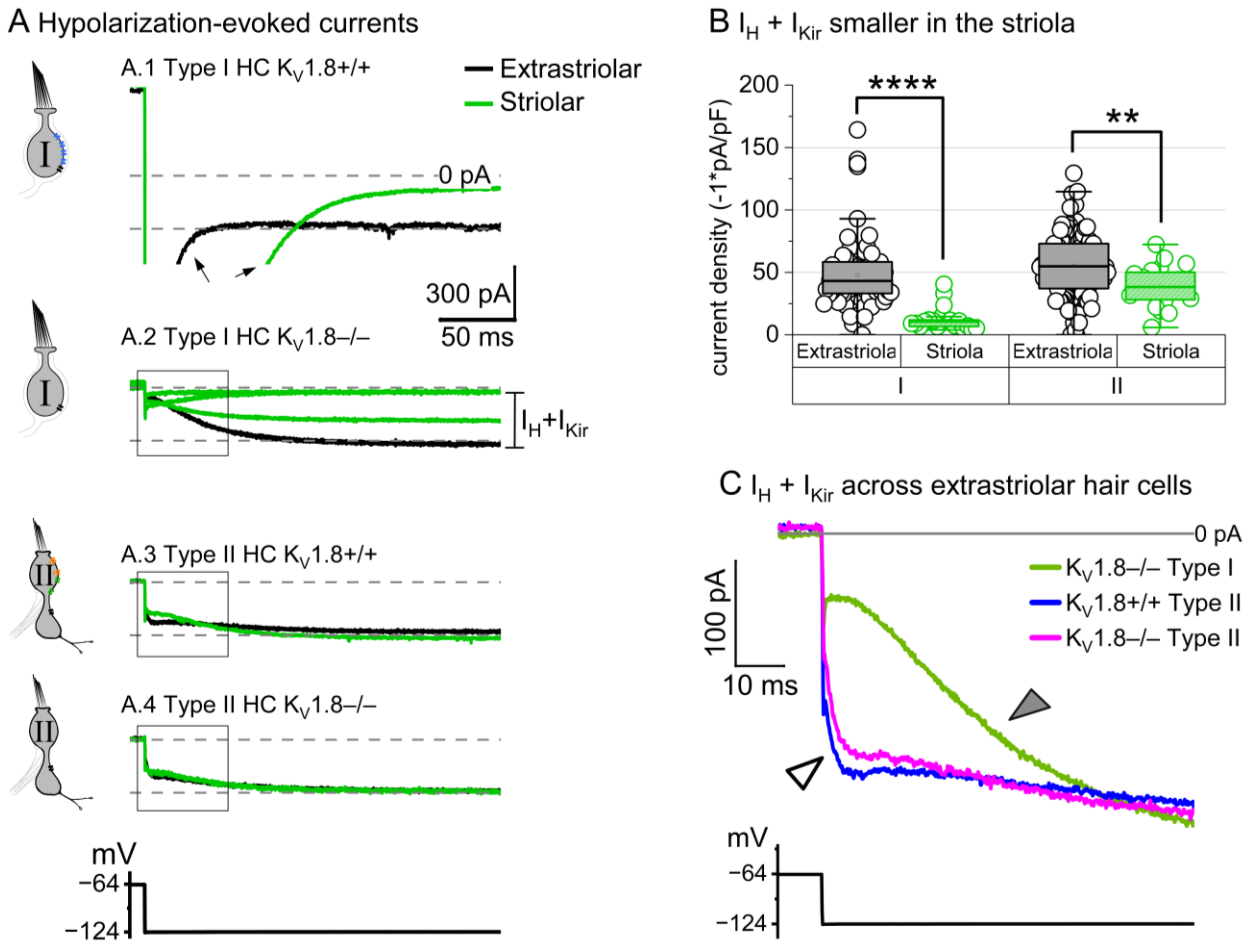

Supplemental Figure 6. No difference was detected in H (HCN) and Kir (fast inward rectifier) currents between $K_V1.8^{+/+}$ and $K_V1.8^{-/-}$ hair cells, consistent with a specific involvement of $K_V1.8$ in *Kcna10* expression.

(**A**) Hyperpolarizing voltage steps evoked I_{Kir} and I_{HCN} in $K_V1.8^{+/+,+/-,-/-}$ type I and II HCs. **A.1** *Arrows*, deactivation of $g_{K,L}$. **A.2-A.4** *Bracket,* the sum of I_H and I_{Kir} were measured as total inward current after 250 ms at –124 mV.

(**B**) Summed I_{KIR} and I_H density was the same across genotypes but smaller in striola than extrastriola (see Supplemental Table 3 for statistics).

(**C**) Inward currents seen at the onset of hyperpolarization, including I_{Kir}, were larger in type II HCs than type I. Magnification of boxed in inset from the extrastriolar cells in A.2-A.4. *Open arrowhead*, activation of fast inward rectifier, I_{Kir}; *filled arrowhead*, slower activation of I_{HCN}.

825
826
827
828

Supplemental Table 1. *Test of sex differences in hair cell K_V channel data.*

Cell Type	Parameter	Subgroup	Male vs Female posthoc p-value	Test
Type I HC	Tail V_{half}	+/+,+/–	0.0023 ** [a]	Normal, homogeneous variance ANOVA: Genotype (2 levels), Sex (2 levels), Zone (2 levels), Genotype*Sex.
		–/–	0.57	
	Tail S	+/+,+/–	0.98	ANOVA: Genotype (2 levels), Sex (2 levels), Zone (2 levels), Genotype*Sex. Normal, homogeneous variance
		–/–	0.58	
	Tail $g_{Density}$	+/+,+/–	0.999	Normal, nonhomogeneous variance Welch ANOVA: Genotype*Sex
		–/–	0.936	
Type II HC	Peak V_{half}	+/+,+/–	0.95	Normal, homogeneous variance ANOVA: Genotype (2 levels), Sex (2 levels), Zone (2 levels), Genotype*Sex.
		–/–	0.28	
	Peak S	+/+,+/–	0.999	Normal, homogeneous variance ANOVA: Genotype (2 levels), Sex (2 levels), Zone (2 levels), Genotype*Sex.
		–/–	0.97	
	Peak $g_{Density}$	+/+,+/–	0.64	Normal, nonhomogeneous variance Welch ANOVA: Genotype*Sex
		–/–	0.43	
	% inactivation at 30 mV	+/+,+/–	0.98	Normal, homogeneous variance ANOVA: Genotype (2 levels), Sex (2 levels), Zone (2 levels), Genotype*Sex.
		–/–	0.82	

[a] g, 0.9. Male $K_V1.8^{+/+,+/-}$, –85 ± 1 mV (40) vs. Female $K_V1.8^{+/+,+/-}$, –79 ± 2 mV (12)

829
830
831
832
833

Supplemental Table 2. *Soma size of type I HCs. The perimeter of cross-sections of basolateral cell bodies was manually measured from immunohistochemistry sections with sufficient autofluorescence in the 488 channel to distinguish cell morphology, and anti-calretinin to label type II hair cells and calyx-only afferents. Cells were measured from two female littermates.*

Cell Type	Genotype	Age	Weight (g)	Perimeter (µm)	Test
Type I HC	+/+	P117	24.9	47 ± 1 (19)	ANOVA: p=0.1, power = 0.07
	–/–	P117	25.2	46 ± 1 (28)	

834

Supplemental Table 3. *Detected zonal but not genotype differences in hair cell I_{Kir} and I_H.*

Cell Type	Zone	I_H + I_{Kir} current density (-1*pA/pF)	$K_v1.8^{+/+,+/-}$ *vs* $K_v1.8^{-/-}$ p-value	ES *vs* Striola p-value	Test
Type I HC	ES Striola	48 ± 3 (78) 13.0 ± 2 (19)	0.3	4E-9 **** [a]	Non-normal, KWA
Type II HC	ES Striola	55 ± 2 (116) 39 ± 4 (20)	0.19 (0.25 power)	0.0058 ** [b]	Normal, homogeneous variance. 2-way ANOVA: Genotype (2 levels), Zone (2 levels)

[a] g 1.4
[b] g 0.6